Contract No:

This document was prepared in conjunction with work accomplished under Contract No. DE-AC09-08SR22470 with the U.S. Department of Energy (DOE) Office of Environmental Management (EM).

Disclaimer:

Evaluation of Shielding Efficacy of a Ferrite Containing Ceramic Material

C. G. Verst

October 2015
SRNL-TR-2015-00244, Revision 0

DISCLAIMER

Printed in the United States of America

Prepared for
U.S. Department of Energy

SRNL-TR-2015-00244
Revision 0

Keywords: *Mitsuishi*
Radiation Shielding

Retention: *Permanent*

Evaluation of Shielding Efficacy of a Ferrite Containing Ceramic Material

C. G. Verst

October 2015

Prepared in conjunction with work accomplished under contract number DE-AC09-08SR22470 with the U.S. Department of Energy (DOE) Office of Environmental Management (EM).

Savannah River National Laboratory™
OPERATED BY SAVANNAH RIVER NUCLEAR SOLUTIONS

REVIEWS AND APPROVALS

AUTHORS:

_____

E.G. Name, Process Technology Programs Date

TECHNICAL REVIEW:

_____

Example Reviewer, Example Organization, Reviewed per E7 2.60 Date

APPROVAL:

_____

Your Manager, Manager Date
Your Manager's Organization

_____

S.L. Marra, Manager Date
Environmental & Chemical Process Technology Research Programs

_____

Your Customer, Manager Date
Customer's Organization

EXECUTIVE SUMMARY

The shielding evaluation of the ferrite based Mitsuishi ceramic material has produced for several radiation sources and possible shielding sizes comparative dose attenuation measurements and simulated projections. High resolution gamma spectroscopy provided uncollided and scattered photon spectra at three energies, confirming theoretical estimates of the ceramic's mass attenuation coefficient, μ/ρ. High level irradiation experiments were performed using Co-60, Cs-137, and Cf-252 sources to measure penetrating dose rates through steel, lead, concrete, and the provided ceramic slabs. The results were used to validate the radiation transport code MCNP6 which was then used to generate dose rate attenuation curves as a function of shielding material, thickness, and mass for photons and neutrons ranging in energy from 200 keV to 2 MeV.

TABLE OF CONTENTS

LIST OF TABLES

LIST OF FIGURES

1.0 INTRODUCTION

A propriety ceramic material fabricated and supplied by the customer, Mitsuishi, has been evaluated for radiation shielding effectiveness. Gamma and neutron dose rate experiments were performed in the Low Scatter Irradiator (LSI) facility operating at Savannah River Site. Penetrating dose rates and particle spectra were measured through the ceramic slabs of varying thickness and compared against the same experimental measurements for concrete, steel, and lead. Radiation transport modelling was then performed using MCNP6 to extrapolate the findings to other source and shield configurations not explicitly tested. The results provide an effective means of identifying, for a given shielding size or cost restraint, the radiation type and energies at which the ceramic shield becomes competitive.

1.1 Background

MATERIAL COMPOSITON, DENSITY, FABRICATION, COST

JAPANESE EXPERIMENTS DONE PRIOR

2.0 OBJECTIVES AND APPROACH

A comprehensive evaluation of the neutron and gamma shielding capability of the Mitsuishi ceramic has been requested. Four physical samples of the material were provided with which to perform lab based experiments. Each sample measured 150mm wide by 150mm tall but featured a different thickenss. The provision of a 20mm, 30mm, 40mm and 50mm thick sample allowed accurate assessment of attenuation coefficents and build up effects which vary with shield depth traversed by radiation particles.

The lab based portion of the evaluation produced experimentally resolved dose rate knockdown factors as a function of shielding thickness for various shielding materials (e.g. Mitsuishi ceramic, stainless steel, concrete, and lead). Multiple gamma energies and a fission neutron spectrum were used to develop these data. High Purity Germanium (HPGE) detector spectra of penetrating photon spectra from two radionuclide sources were also obtained for the ceramic material and used to confirm flux attenuation rates.

The experimental tests were simulated using MCNP6, an industry standard radiation transport code. Validity of the code and its treatment of the custom Mitsuishi ceramic material were demonstrated through comparison of the modeled results to the experimental data. MCNP6 was then used to represent numerous radiation transport models designed to assess the dose shielding effectiveness of each considered material for several radiation source configurations. The use of dosimetric modelling allows rapid acquisition of bulk data which can be used to target specific shielding applications for which the material seems well suited.

3.0 GAMMA SPECTROSCOPY

High resolution gamma spectra were taken to assess the flux response through the provided Mitsuishi ceramic shielding samples. Two sealed radionuclide sources, Cs-137 and Co-60, were utilized to provide attenuation rates at multiple photon energies. Cs-137 emits a 661.7 keV photon immediately following a beta decay to Ba-137m. Co-60 emits two photons with equally high probability at 1173 keV and 1333 keV. Because photon interaction probabilities and mechanisms depend on incident photon energy, it is important to observe the effects of the shielding material at multiple energies. These nuclide sources cover the energy range of interest for most shielding applications and are themselves typically the dominant sources of dose in many cases.

Spectral measurements were taken using a Falcon 5000 high purity germanium (HPGE) detector using Genie 2000 acquisition software. The calibrated detector was instructed to record data for a live time of 300 seconds for each measurement. Live time measurements ensure that the dead time of the detector caused by internal electronic limitations in high flux fields does not reduce the total number of detectable photon interaction events. This allows a direct comparison of shielded and unshielded flux.

3.1 HPGE Measurements

The HPFE detector was placed near the edge of a table, one meter above ground, such that most exposed face of the semiconducting crystal was facing off the table. Spectral measurements were taken without any source or shield present to establish a radiation background and confirm that there will be no interference at the photon energies being tested. The resulting spectrum is shown in Figure 1below.

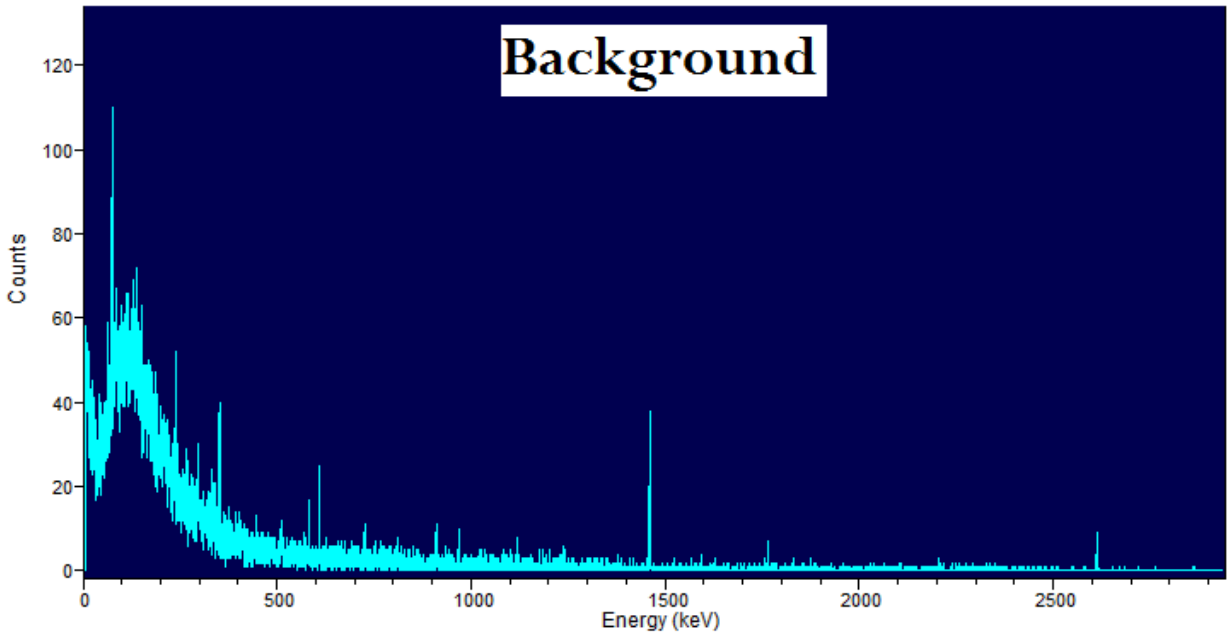

Figure 1. Background Gamma Spectrum as Measured by Falcon 5000 HPGE Detector

The photopeaks at 1460 keV and 609 keV are from K-40 and Bi-214 respectively, naturally occurring radiological material (NORM) which is effectively ubiquitous. These peak energies are highly distinguishable from the radionuclide energies of Cs-137 and Co-60 when using an HPGE semiconductor detector and so do not present an issue for detection. Note that the count rates for these NORM are also very low when compared to the activity of the nuclide source used to evaluate flux and dose attenuation.

Following background measurements, a .044 mCi Cobalt-60 source was suspended 1 meter above ground directly in line with the center of the front face of the detector. The distance between the face of the detector and the source was 88 cm. Because the detector crystal is actually inset ~2 cm from the face, the source to detector distance may be approximated as 90cm. A 300 second live time count was record for this configuration and represents the baseline, unshielded spectra of a Cobalt-60 source. Each of the four shielding samples were then introduced individually in order to obtain a resultant flux spectrum through 20mm, 30mm, 40mm, and 50mm of the ceramic shielding. The ceramic shielding samples were placed 3 cm in front of the detector face (~5cm from the crystal) as indicated in Figure 2

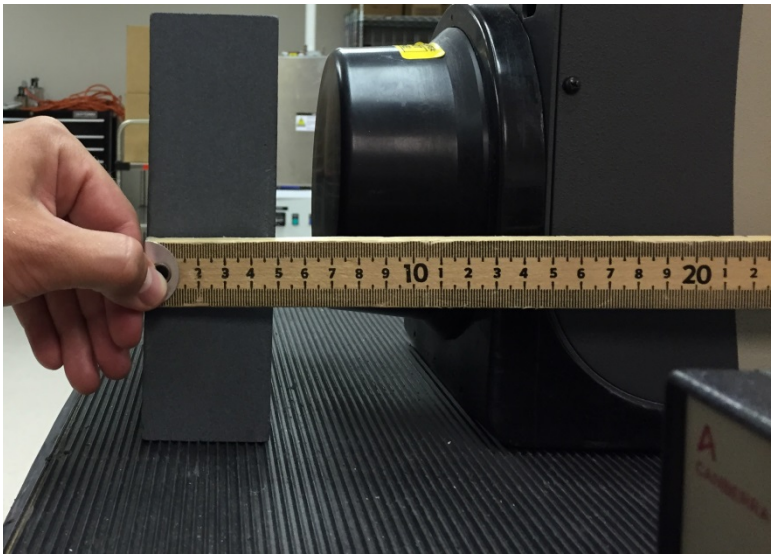

Figure 2. Setup For HPGE Shielded Measurements

The resulting gamma spectrum shows an expected decline in total counts within the photopeak regions of interest for the nuclides tested. Figure 3 focuses on the 1.17 MeV gamma line of Co-60. The total counts for the unshielded experiment are represented by the light blue line while the dark blue line reveals the drastic reduction in uncollided flux caused by the 50 mm ceramic shield. Measurements through each shield were repeated for a .99 mCi Cs-137 source.

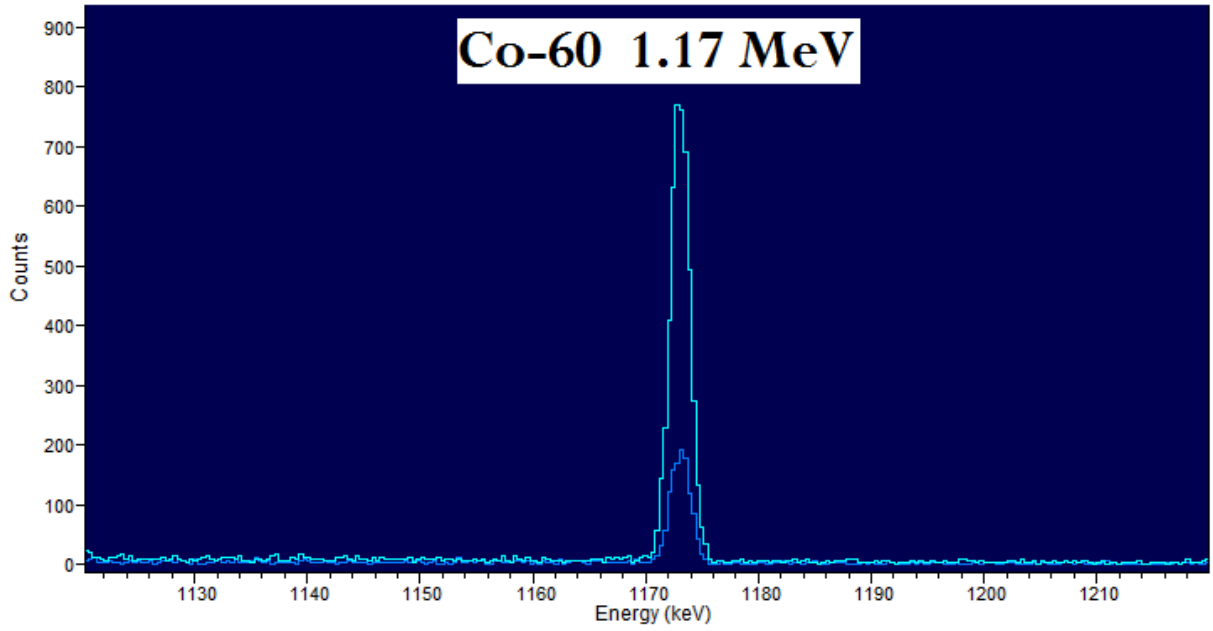

Figure 3. HPGE Spectra of Co-60 1.17 MeV Peak – Unshielded (Light Blue) & 50mm Shielded (Dark Blue)

3.2 Calculation of Attenuation Coefficient

Once spectra were obtained for both radionuclides sources and for 0, 20, 30, 40, and 50 mm of shielding, the spectrum analyzing software Genie 2000 was employed to characterize each peak and calculate integral counts, a measure of uncollided intensity for that energy. The results of the measured counts are

listed in Table 1 and normalized to the counts of the unshielded case in order to determine the attenuation of uncollided intensity.

Table 1: Photopeak Integral Counts

Attenuation Thickness (cm)	Raw Counts (Intensity, I)			Normalized Counts (I/I_0)		
	1173 keV	1332 keV	662 keV	1173 keV	1332 keV	662 keV
0	$4.63x10^3$	$4.11x10^3$	$3.02x10^5$	1	1	1
2	$2.62x10^3$	$2.34x10^3$	$1.44x10^5$	0.5659	0.5693	0.4768
3	$1.97x10^3$	$1.82x10^3$	$9.86x10^4$	0.4255	0.4428	0.3265
4	$1.56x10^3$	$1.49x10^3$	$7.30x10^4$	0.3369	0.3625	0.2417
5	$1.18x10^3$	$1.11x10^3$	$4.91x10^4$	0.2549	0.2701	0.1626

Monoenergetic photon attenuation rates can be predicted by the linear attenuation coefficient, μ, which describes the probability of photon interaction per unit distance travelled. The fraction of surviving, uncollided photons which traverse a shielding distance, x, can be described by Equation 1.

Equation 1

$$\frac{I}{I_0} = e^{-\mu x}$$

The knockdown factors determined in Table 1 can then be used to calculate attenuation coefficients for the ceramic material of 0.365 cm^{-1}, 0.278 cm^{-1}, and 0.267 cm^{-1} at energies of 662 keV , 1173 keV, and 1332 keV respectively. A comparison of these experimental results against the theoretical attenuation coefficient can be performed if the weight percent of each constituent element in the material is known. A plot of the theoretical attenuation coefficient of the ceramic material is provided in Figure 4 along with the three experimentally obtained values at the discrete energies tested. The explicit calculation of the theoretical data is not included in this report so as to respect the proprietary nature of the material's composition. It is clear that the attenuation coefficient calculated from the gamma spectroscopy matches extremely well with the theoretical values expected for the energies considered, lending credibility to the HPGE spectra.

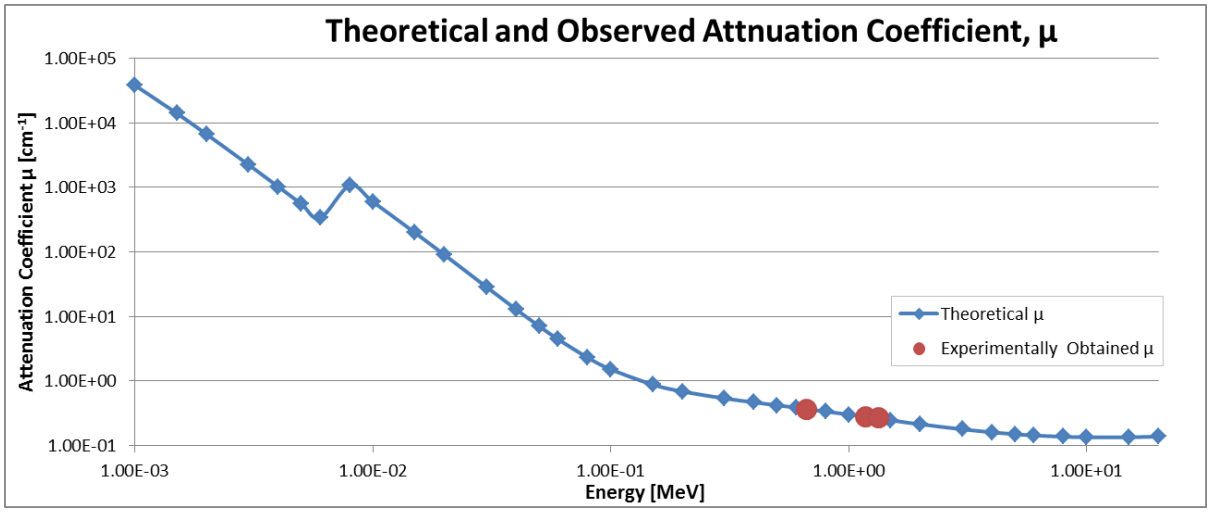

Figure 4. Theoretical Attenuation Coefficient, μ, Based upon Known Elemental Composition, and Density, Overlain with Experimentally Resolved μ

Unfortunately, the attenuation coefficient discussed here does not completely describe the energy loss mechanisms and is therefore not sufficient enough to predict penetrating dose. Gamma energy deposition depends upon the specific type of interaction between the photon and the target matter. This, in turn, varies with the energy of the incident photon. In addition to the uncollided photon fluence, which has now been described in magnitude and energy, there is also a substantial amount of penetrating secondary radiation, (e.g. photoelectrons, Bremsstrahlung X-rays, Compton scattered photons) which contribute to the dose in the target. Due to the difficulty of describing energy, momentum, and direction through a function of time and space in a heterogeneous environment, the estimation of dose relies instead on empirically determined values for radiation buildup, deterministic simulation via modelling codes, or physically performing the irradiation and extrapolating to cases of interest. The first method cannot be utilized because buildup factors for this material have not yet been measured for any shielding configuration. However, the latter two methods are both performed as part of the present evaluation and described throughout this report.

4.0 DOSIMETRY

Penetrating dose was experimentally measured through the ceramic shielding material using the Low Scatter Irradiator (LSI) system developed by Hopewell Designs and operated by the Savannah River Site. The facility features a large cubic room with a pneumatic source tube used to elevate high activity radionuclide sources to the central exposure position 20 feet from the walls, floor and ceiling. Four independently movable detector platforms can be remotely driven along tracks that extend radially from the source position. The entire construction of the massive irradiation chamber is designed to minimize scattered radiation contributions from anything not intentionally placed between the source and detector(s). Note that the grate supporting the detector tracks shown in Figure 5 is actually 20 feet above the concrete floor of the room.

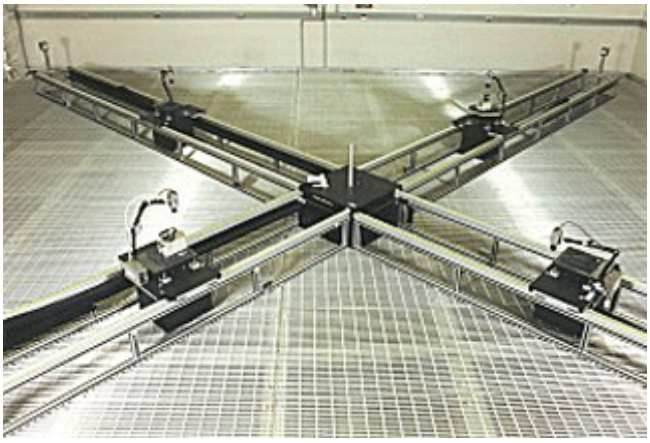

Figure 5. Model N40 Low Scatter Irradiator (Hopewell Designs Inc.)

Cs-137 and Co-60 were once again used as photon sources, and Cf-252 was used as a source of spontaneous fission neutrons. Dose rate detectors were placed on each of the four tracks at a distance of 74 cm from the source locations. This distance was chosen to provide a balance between obtaining good counting statistics over reasonable count times without oversaturating the detectors for all three sources available. A custom sample holder was used to secure the four ceramic slabs at the appropriate height and distance from the source during exposure.

4.1 Gamma Dose Rate Measurements

RO-20 Iron Chamber Survey Meters were used for detection of photon dose rate. The RO-20 dose rate meter displays dose in real time. Dose rates were recorded after 30 seconds once the instrument readings reached steady state. Redundant background measurements and baseline (unshielded) measurements were taken with each detector to ensure consistency between the instruments. The ceramic samples were then loaded on the sample rack and four simultaneous dose rate readings were recorded through the four ceramic plate of various thickness. Figure 6 shows the experimental set up for simultaneous dose rate measurements through all four ceramic shields. The radionuclide source travels up to the level of the detectors through a tube centered between the ceramic shields.

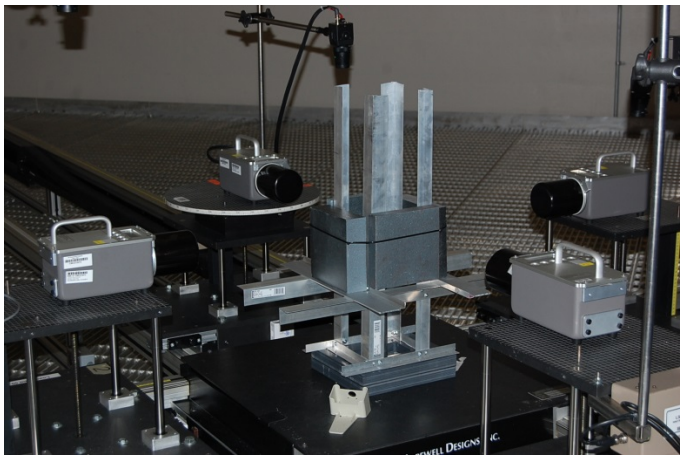

Figure 6. Shielded Source Dose Rate Experiment Performed in the LSI

These tests were done for a 1.63 Ci Co-60 source and a 70.8 Ci Cs-137 source. Additionally, stainless steel, lead, and concrete bricks were each test to provide comparison points against the ceramic samples. The results of the gamma dose rate tests appear in Table 2.

4.2 Neutron Dose Rate Measurements

Neutron detection is somewhat more difficult that photon detection, and exact dose rate measurements can vary between detector types, thus requiring extensive calibration and application of response functions to reach agreement. The instruments used for this evaluation were Rem500 models which have been identically calibrated for use in the LSI so as to provide uniform dose response.

A 0.23 Ci Cf-252 was used as the neutron source due to its high spontaneous fission rate. Fission neutrons are emitted at a range of energies which follow a well-known distribution. This distribution is fairly consistent among all fission sources, but it is important to note that neutron interaction rates depend heavily on the incident neutron energy and that the neutron dose attenuation measured in this experiment applies only to the fission neutron spectrum, not necessarily all discrete neutron energies.

The testing setup for neutron dose was identical to that of gamma dose, but the instruments were operated in “integrate mode” rather than “rate mode” due to the low counting efficiency of neutron detectors which lead to fluctuating real-time dose rates. Counting in integrate mode simply monitors the total amount of energy deposited (dose) in the detector. Dividing this value by the 10 minute exposure time for each test yields an average dose rate. The results of the neutron dose rate tests appear in Table 2

Table 2: Gamma and Neutron Dose Rate Measurements

Shielding Material	Thickness	Cs-137 Dose Rate	Co-60 Dose Rate	Cf-232 Dose Rate
	(mm)	(R/hr)	(R/hr)	(R/hr)
Bare	0	43.5	3.5	1.55
Ceramic	50	13.9	1.4	1.7
Ceramic	40	17.5	1.7	2
Ceramic	30	22.5	2.1	2.2
Ceramic	20	29	2.5	2.4
Stainless Steel	50.8	5	0.7	1.05
Lead	50.8	0.7	0.2	1.35
Concrete	47.5	27	24	1.55

4.3 MCNP Results Verification

The physical experiments performed to assess the ceramic material's attenuation coefficient and dose shielding efficacy provide authentic, indisputable results from which comparisons can be made and conclusions drawn. However, the scope of consideration is somewhat limited to the radiation sources and shielding configurations tested, and it quickly becomes onerous attempting to test all possible applications. It is therefore advantageous to employ modelling and simulation to extrapolate the laboratory findings to scenarios not explicitly tested. Therefore, the present evaluation includes MCNP6 simulations of a wide variety of shielding configurations with which to compare different materials' shielding performance.

4.3.1 Calculation Tools and Quality

The Monte Carlo N-Particle transport code version 6 (MCNP6)[1, 2] was used to perform shielding modelling and energy deposition calculations. MCNP6 is a general purpose Monte Carlo code that can be used for neutron, photon, electron, or coupled transport. It is used to calculate position-dependent radiation flux and resultant effective dose rates for any user specified geometry and source definition. MCNP6 is an industry standard software package that is widely used and thoroughly benchmarked for radiation transport calculations.

4.3.2 LSI Simulation

The experiments performed in the LSI were modelled in MCNP6 and the resulting dose rate attenuation rates were compared between the simulation and experimental observation. A successful comparison indicates that the physics treatment utilized by MCNP6 is accurate for the materials and radiation being considered. This helps to verify the integrity of future models. Two dimensional representations of the MCNP6 model used are provided in Figure 7.

[1] LA-UR-03-1987, MCNP – A General Monte Carlo N-Particle Transport Code, Version 5, X-5 Monte Carlo Team, April 24, 2003 (Revised 10/03/05)LA-CP-13-0643, MCNP6 User's Manual, Monte Carlo Team, May, 2013.

[2] LA-CP-13-0643, MCNP6 User's Manual, Monte Carlo Team, May, 2013.

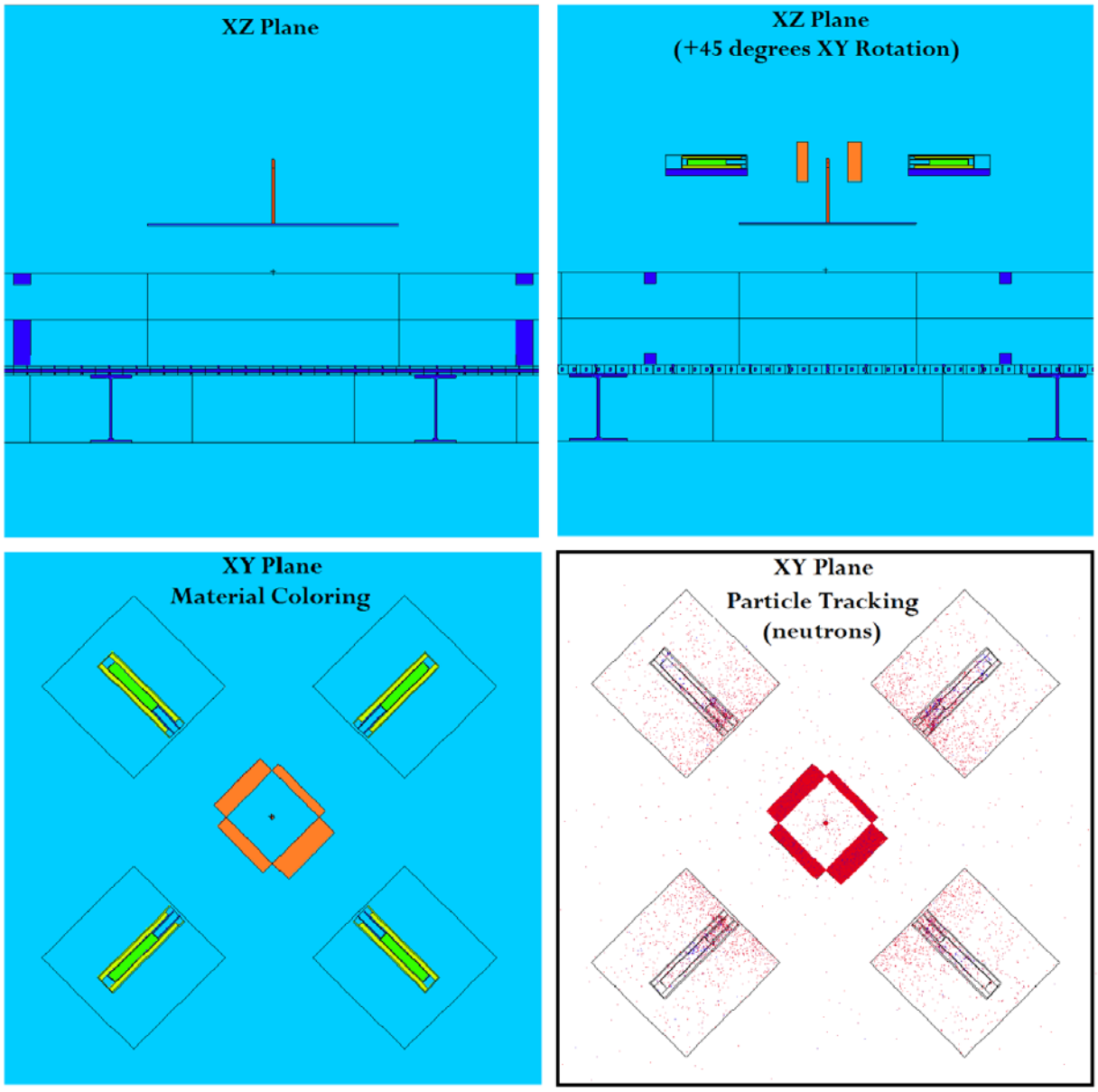

Figure 7. MCNP Model of LSI Dose Rate Experiments

Models were created for all dose rate experiments tested in the LSI. The simulated shielded dose rates projected by MCNP models are plotted along with corresponding attenuation curves measured in the LSI in Figure 8. A comparison reveals excellent agreement between the measured dose rates and simulated predictions. It is worth noting that the unusual attenuation trend found in both the measured and modelled neutron experiments is due to the strong scatter effect of neighboring ceramic samples. When one sample is tested at a time, it was proven the dose rate does indeed fall off more rapidly through the first 2 centimeters of shielding. When all samples are exposed simultaneously, neutron scatter events, especially from the neighboring thick slabs, redirect additional fluence to the other slabs. This is not an unexpected behavior, and the fact that MCNP corroborates the trend further suggests that the code features accurate neutron transport simulation.

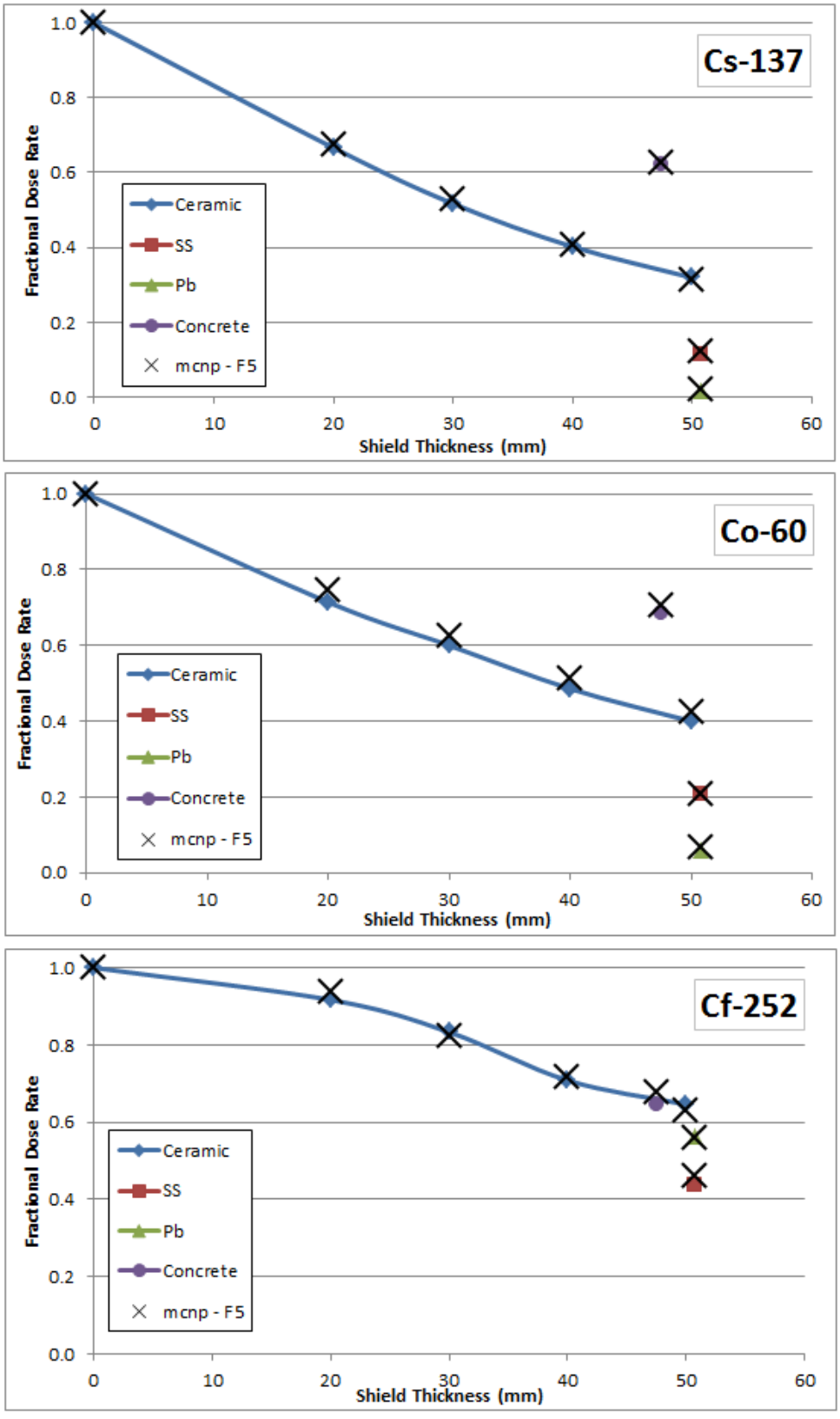

Figure 8. Fractional Dose Rate as Measured by RO-20 (gamma), Rem500 (neutron), and MCNP6

5.0 Further Modelling

5.1 Spherical Shield Configuration

Following the confirmation of MCNP results, several additional models were created to estimate dose rates for many combinations of radiation energies and shielding thickness. A simple spherical geometry was initially chosen for these simulations in order to capture the most conservative estimates of dose penetration. Each model consists simply of a point source of a specified radiation particle type and starting energy. The point source is surrounded by a sphere of shielding material, also of a specified thickness ranging from 1 cm radius to 15 cm radius. A spherical surface surrounds the shielded source at 32 cm and measures the passing flux as a function of particle energy. This configuration ensures that the detector obtains a contribution from all penetrating radiation. Figure 9 shows the spherical shield configuration as well as simulated photon particle tracks through a stainless steel shield.

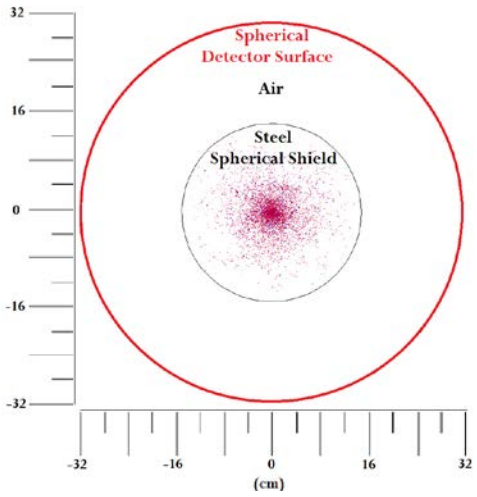

Figure 9. Spherical Shield Configuration - MCNP

ANSI 1977 fluence-to-dose conversion factors are used to energy weighted fluence rates to tissue dose rates. These dose rates were tallied for neutron and photon energies between 200 kev to 2 MeV at 200 keV intervals. Five different shielding materials were tested; the Mitsuishi ceramic, lead, stainless steel, concrete, and aluminum. For each material tested, the shield thickness varied between 1cm and 15cm to provide fractional dose rates as a function of shield thickness for 5 materials simultaneously. The resulting dose rates have been normalized to the unshielded values for ease of comparison. Normalized penetrating dose is tabulated for 1 MeV photons and neutrons in Table 3.

Table 3: Normalized Penetrating Dose for 1 MeV Photons and Neutrons

Normalized Dose - 1 MeV Photon																
Shield thickness [cm]	0	1	2	3	4	5	6	7	8	9	10	11	12	13	14	15
Mitsuishi	1.00	0.91	0.82	0.73	0.65	0.57	0.50	0.44	0.38	0.33	0.28	0.24	0.21	0.18	0.15	0.13
SS	1.00	0.86	0.72	0.59	0.48	0.38	0.30	0.24	0.19	0.15	0.11	0.09	0.07	0.05	0.04	0.03
Lead	1.00	0.73	0.51	0.34	0.23	0.15	0.10	0.06	0.04	0.03	0.02	0.01	0.01	0.00	0.00	0.00
Concrete	1.00	0.96	0.91	0.87	0.82	0.78	0.74	0.70	0.66	0.62	0.59	0.55	0.52	0.49	0.45	0.42
Aluminum	1.00	0.95	0.90	0.85	0.81	0.76	0.72	0.67	0.63	0.59	0.55	0.51	0.48	0.44	0.41	0.38
Normalized Dose - 1 MeV Neutron																
Shield thickness [cm]	0	1	2	3	4	5	6	7	8	9	10	11	12	13	14	15
Mitsuishi	1.00	0.95	0.91	0.88	0.85	0.83	0.80	0.78	0.75	0.72	0.69	0.66	0.62	0.59	0.56	0.52
SS	1.00	0.96	0.92	0.89	0.86	0.84	0.82	0.79	0.78	0.76	0.74	0.73	0.71	0.70	0.69	0.67
Lead	1.00	0.99	0.99	0.98	0.98	0.97	0.97	0.96	0.95	0.95	0.94	0.94	0.93	0.92	0.92	0.91
Concrete	1.00	0.95	0.89	0.83	0.77	0.71	0.64	0.58	0.52	0.47	0.42	0.37	0.32	0.28	0.25	0.22
Aluminum	1.00	0.99	0.99	0.98	0.97	0.97	0.96	0.95	0.94	0.93	0.93	0.92	0.91	0.90	0.89	0.87

The results are also co-plotted for each source energy to allow visual comparison of the potential materials' effectiveness in an identical rad field. Examples of these plots are given in Figure 10 below. The remaining data for other source energies are provided as an attachment to this report.

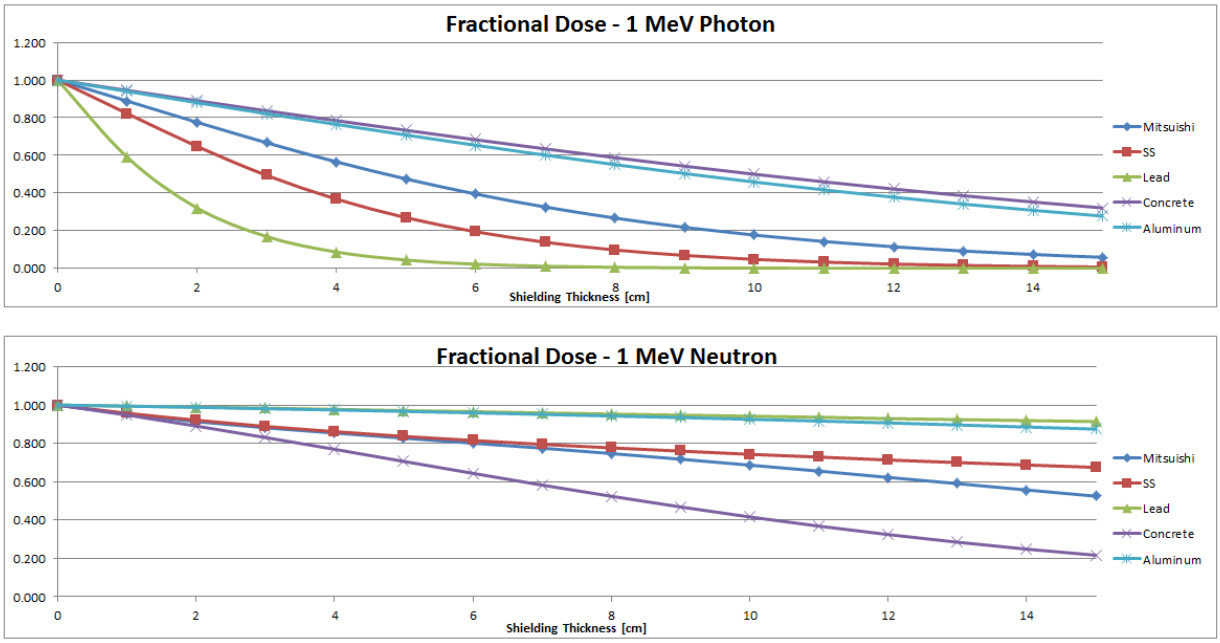

Figure 10. Fractional Dose Rate Attnuation as a Function of Spherical Shielding Thickness

In general, the dose rate simulations suggest that the Mitsuishi ceramic performs better than aluminum and concrete against photons, but is less effective than steel and lead. This is not surprising as photon attenuation scales with the material's atomic number and electron density. Neutron attenuation rates, however, fluxuate dramatically due to highly dependent cross sections. Like photons, neutron transport involves scattering and absorption events, but the relationship between these rates and the incident radiation energy appears much more random and is wildly dissimilar between elements and even isotopes. This leads to less predictable attenuation trends as a function of energy and encourages independent examinations at each energy before making sweeping conclusions. However, concrete seems to be the only material to consistently outperform the Mitsuishi ceramic in terms of dose attenuation as a function of shielding thickness for all starting neutron energies. Stainless steel begins to compete with the ceramic at fast neutron energies (>1 MeV).

In many cases, it will be worth evaluating the materials as a function of required mass rather than shielding thickness, as that will likely be the driving factor of cost and suitability in many applications. Assuming typical densities of the materials considered, the conversion has been made to plot the dose rates from Figure 10 as a function of total shielding mass in Figure 11 rather than thickness. Note how the difference in material densities distinguishes the ceramic's performance against steel for 1 MeV neutrons in applications where mass, not volume, is the limiting factor. Concrete of course excels for neutron applications in which mass is of primary concern due to the high hydrogen and oxygen content.

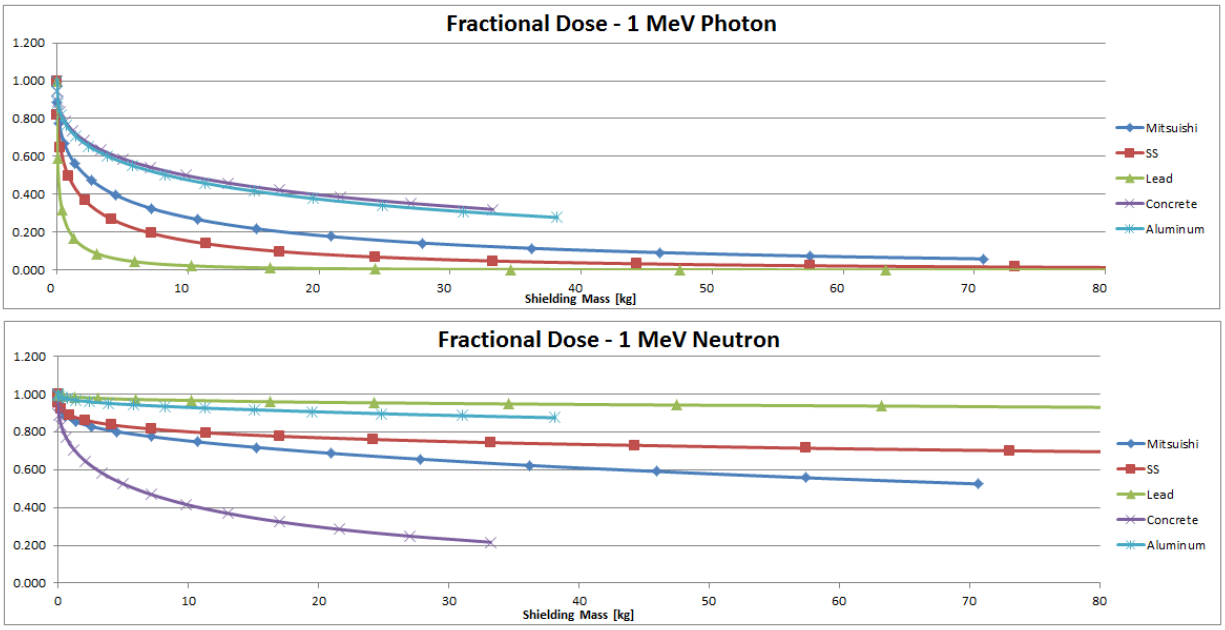

Figure 11. Fractional Dose as a Function of Spherical Shielding Mass

5.2 Slab Shield Configuration

While the spherical shield configuration provides the most comprehensive and conservative estimate of penetrating dose, the majority of shielding applications will not feature complete symmetry and will not consider dose detection at all points equidistant around the source. Many scenarios may only require a shielded slab or wall to one side of the source or a significantly greater distance between the source and shield. These geometric considerations can impact the comparative dose rates, especially with neutrons for which each material possesses significantly different rates of scatter and absorption.

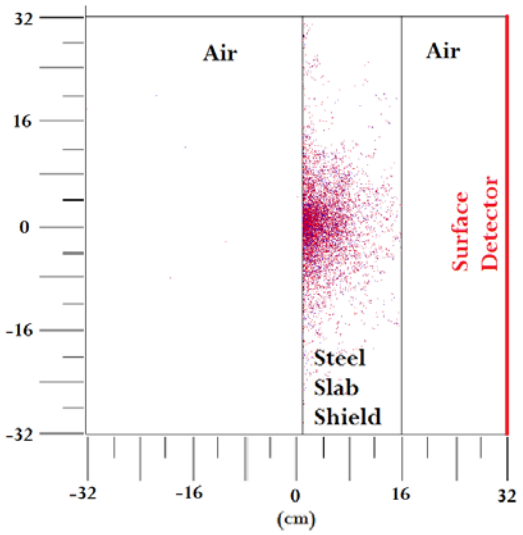

Figure 12. Slab Shield Configuration - MCNP

As an example, consider the configuration where our photon/neutron point source is only shielded on one side by a variably thick slab, and a single detector face is placed 32 cm away. This geometry, illustrated in Figure 12, represents a theoretical counterpart to the spherical shield geometry. The results, plotted in Figure 13, indicate a rather altered comparison in which the ceramic material actually performs better than concrete for the first few centimeters. Additionally, lead and aluminum, which both possess low cross sections, actually appear to increase the measured dose rate for thin shield configurations. This is due to the scattering of angled radiation that would otherwise not have had a direct path to the detector in the absence of any shield. The existence of a thin shield redirects some radiation to the detector without significantly reducing the overall flux through absorption, thereby depositing more energy at the detector location.

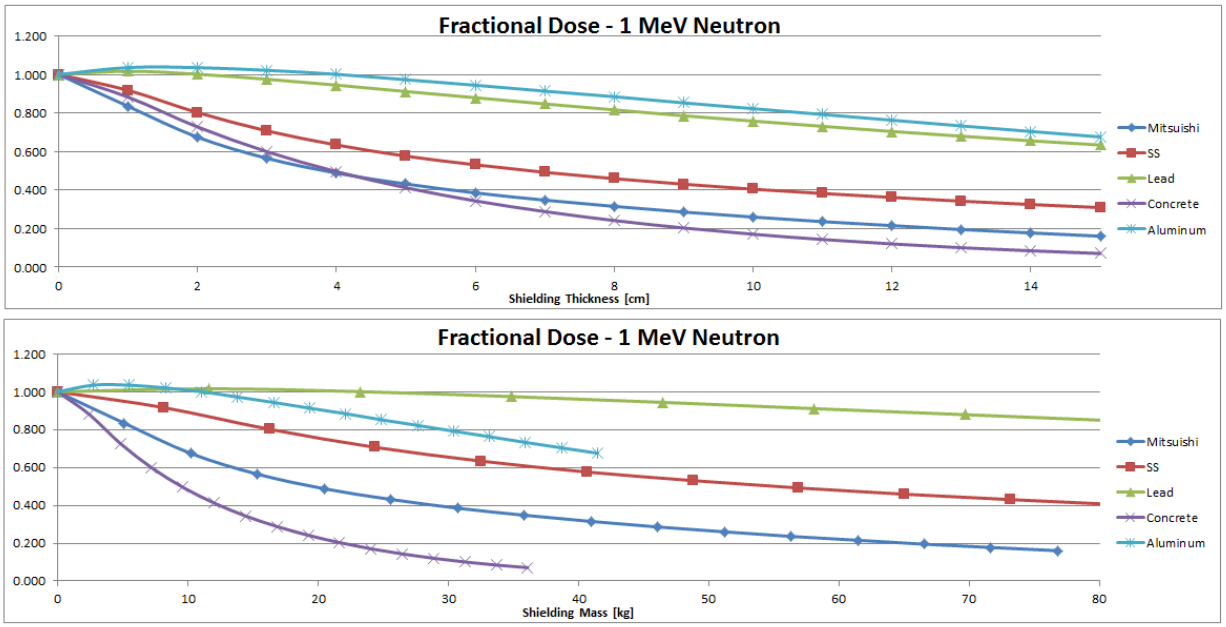

Figure 13. Neutron Fractional Dose through Single Shielding Slab in Air as a Function of Thickness (Top) and Mass (Bottom)

It is clear that the effect that radiation scattering and eventual absorption has on dose rate is dependent on shielding geometry and detector positioning, particularly for neutrons. The single sided slab shield, flat face detector configuration represents perhaps the extreme opposite of the spherical shield configurations. As the source becomes more completely encased in shield or scattering media, the resulting dose rate attenuation curves will tend more towards the spherical shield estimates. It is therefore expected that realistic shielding configurations will result in attenuation curves which fall between the two estimates. While the exact dose rates are hard to predict without specific geometries to model, the relative material rankings are still fairly consistent regardless of shielding configuration.

6.0 Conclusion

Analysis of the dose attenuation curves reveals that the ferrite compound being tested is expectedly less effective than steel or lead at shielding photons of all energies. Comparing attenuation rates is most easily done by visually assessing the curves provided for each energy in the appendix of this report. However, an approximate quantitative comparison can be made using an empirically averaged value which we will call μ' which describes the rate of penetrating dose reduction as a function of shield thickness. These values would be similar to attenuation coefficients for uncollided flux but reflect the effects of buildup for a given geometry and are therefore not valid for very thin/thick shields or for configurations other than source of the empirical data. This rough approximation of the photon results reveals that for moderate to high energy photons (800 keV – 2 MeV) the Mitsuishi ceramic reduces penetrating dose about 25% as effectively as lead and 60% as effectively as steel. Note that the effect is exponential with shielding thickness as described in Equation 2.

Equation 2

$$Dose_{ceramic}(x) = Dose_{lead}e^{\cdot 25x} = Dose_{steel}e^{-.6x} \qquad where\ x\ is\ in\ cm$$

For more accurate photon shielding comparisons, specifically for low energies and thin/thick shields, it is strongly suggested that the provided tables and plots be evaluated individually.

Neutron dose rates vary uniquely for each material as a function of energy and shielding thickness which disallows a blanket comparison. Furthermore, the importance of neutron scattering may preclude extrapolation of two simple geometries modeled as part of the present evaluation to realistic configurations. Fortunately, neutron shielding applications are few and relatively unvaried, thereby limiting the number of scenarios which need to be modeled. Moreover, the simulations that were performed, while not absolutely comprehensive, still provide some conclusive results which can serve to narrow the scope of future evaluations. Concrete and steel are likely to represent the competition for neutron shielding structures. The degree to which the ferrite ceramic contends with these materials for a given energy, mass, and volume was made clear through this evaluation. The disparity between spherical shield and slab shield effectiveness has also highlighted the material's high scattering rates and potential utility in non-uniform shield applications. And while the relative material effectiveness in a neutron field is shown to depend somewhat on geometry, the two theoretical models used for this evaluation are expected to bound any real-world geometries.

Gamma Dose_vs Shield Thickness

200 keV Source

SPHERICAL GEOMETRY

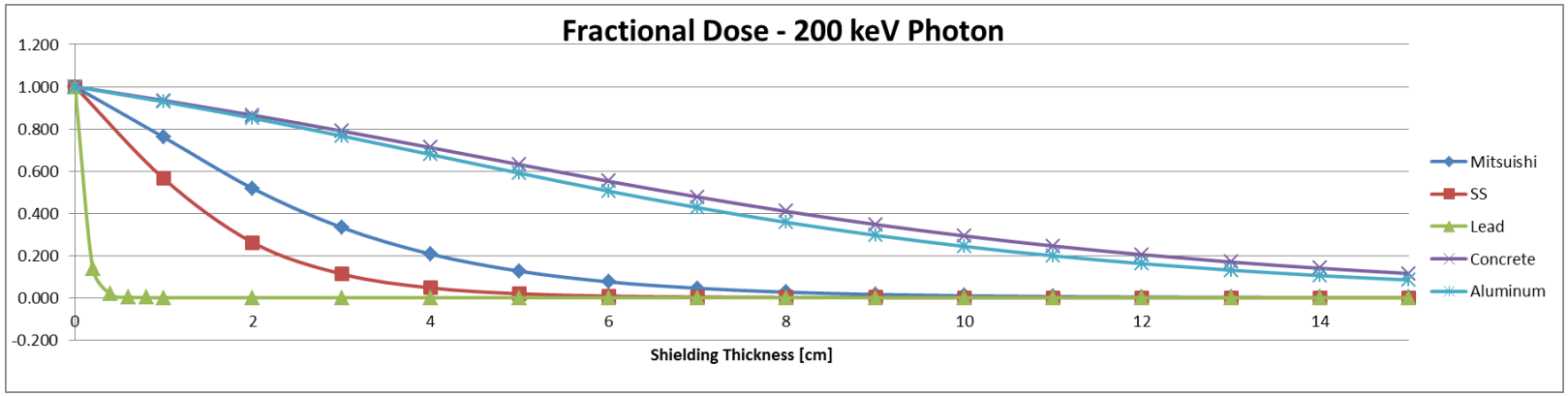

SLAB GEOMETRY

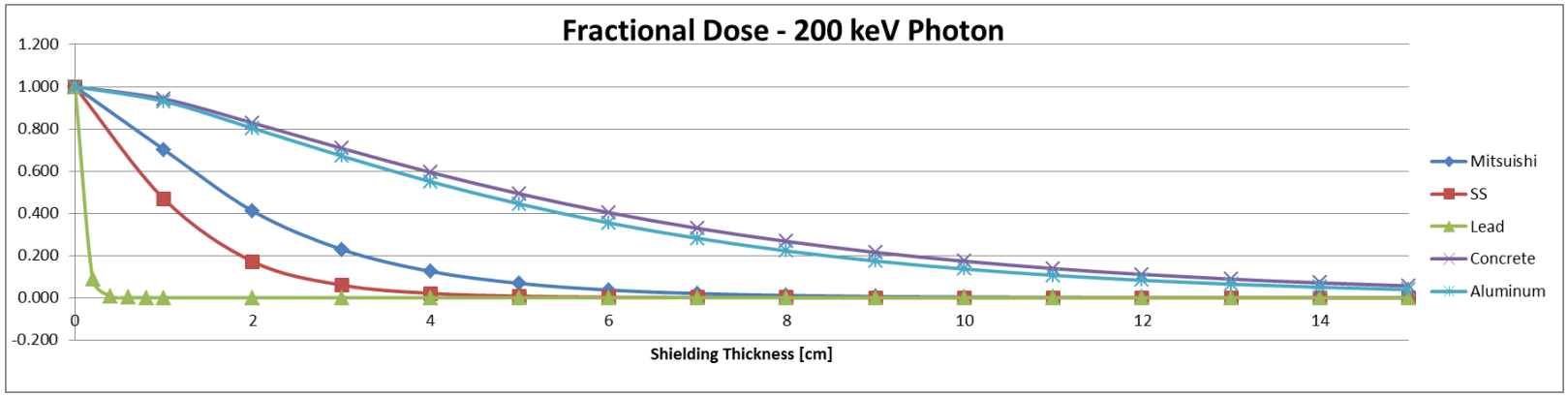

Gamma Dose_vs Shield Thickness

400 keV Source

SPHERICAL GEOMETRY

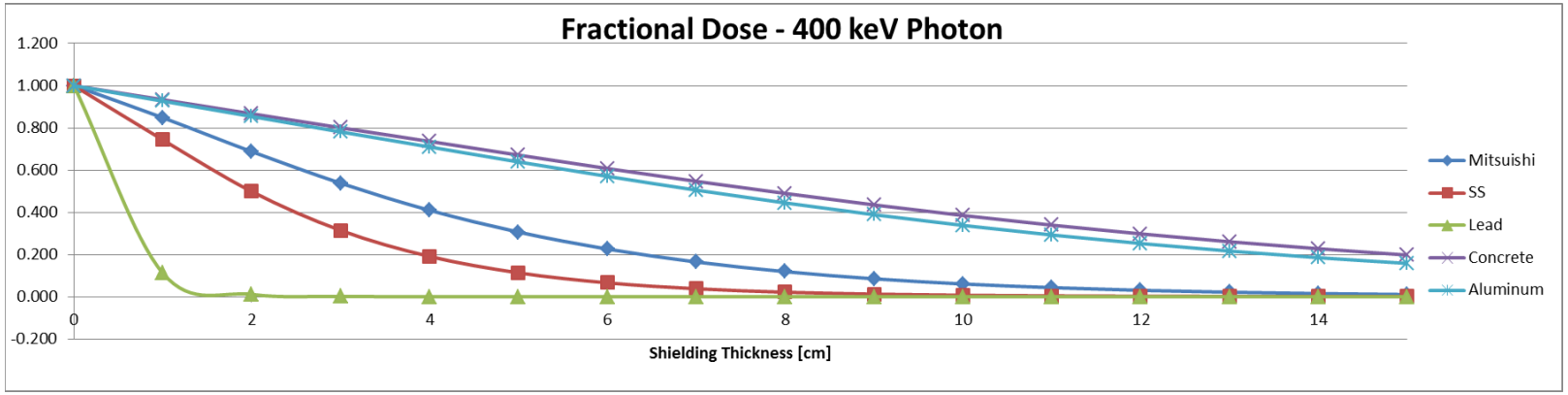

SLAB GEOMETRY

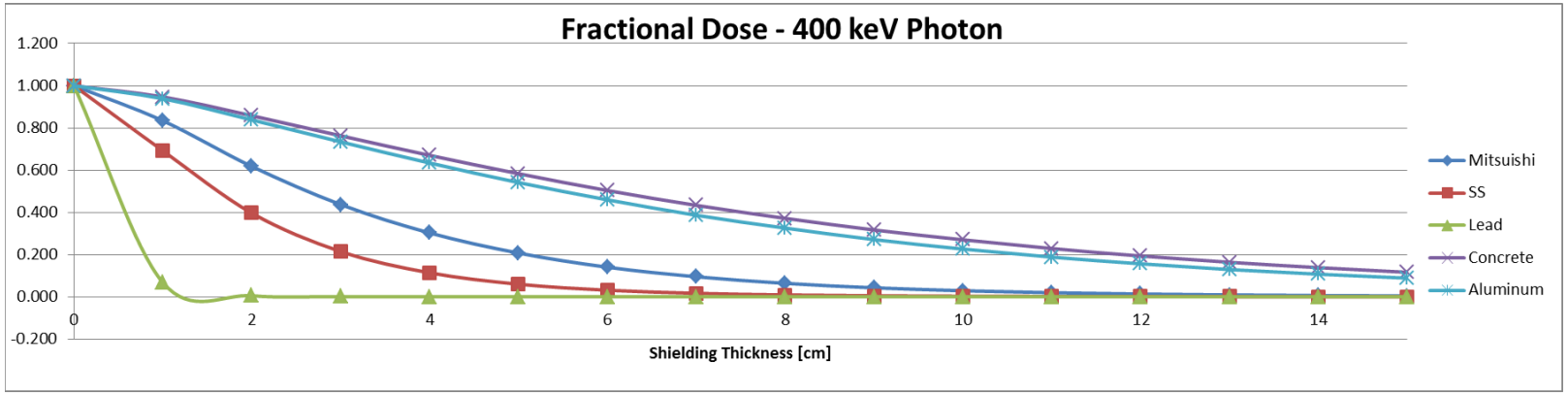

Gamma Dose_vs Shield Thickness_

600 keV Source

SPHERICAL GEOMETRY

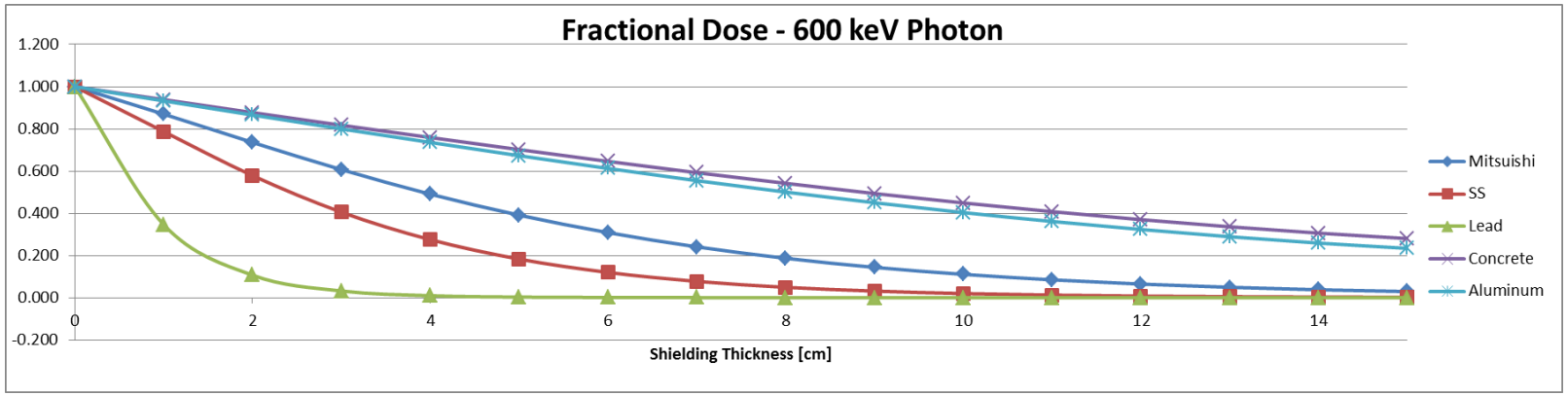

SLAB GEOMETRY

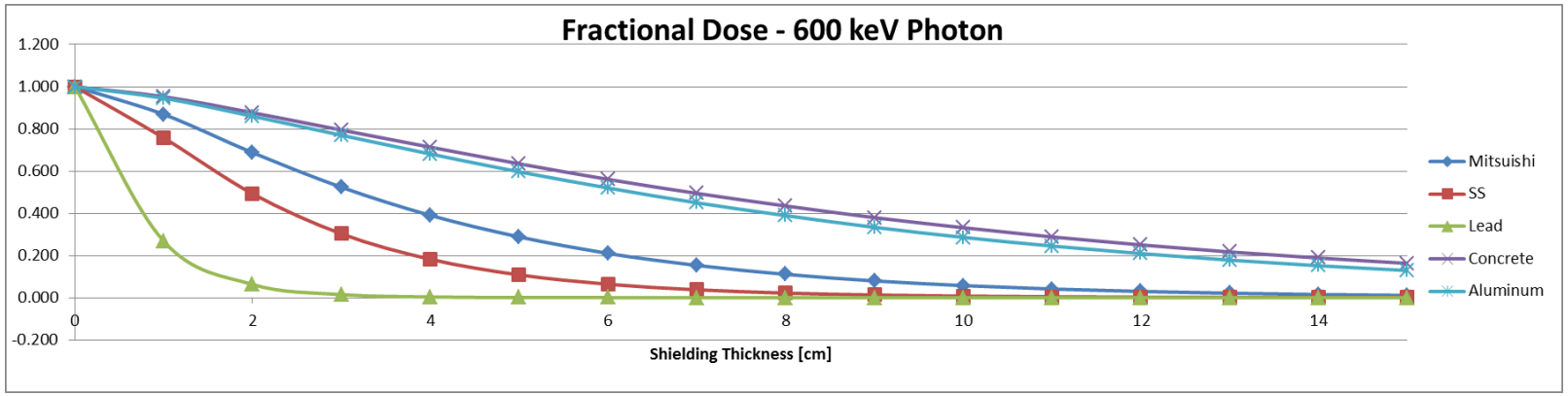

Gamma Dose_vs Shield Thickness_

800 keV Source

SPHERICAL GEOMETRY

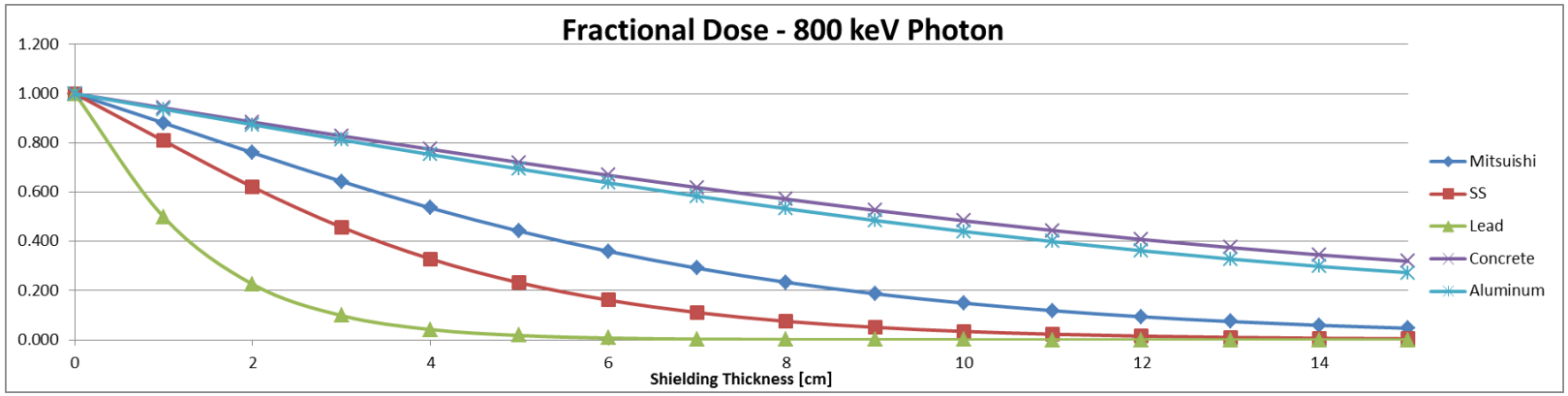

SLAB GEOMETRY

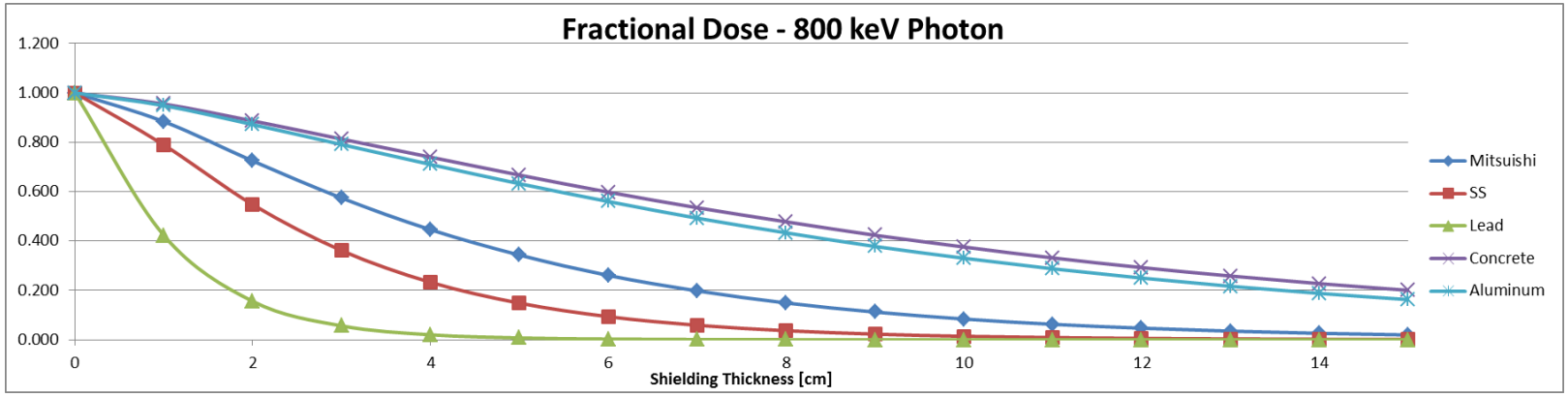

Gamma Dose_vs Shield Thickness

1 MeV Source

SPHERICAL GEOMETRY

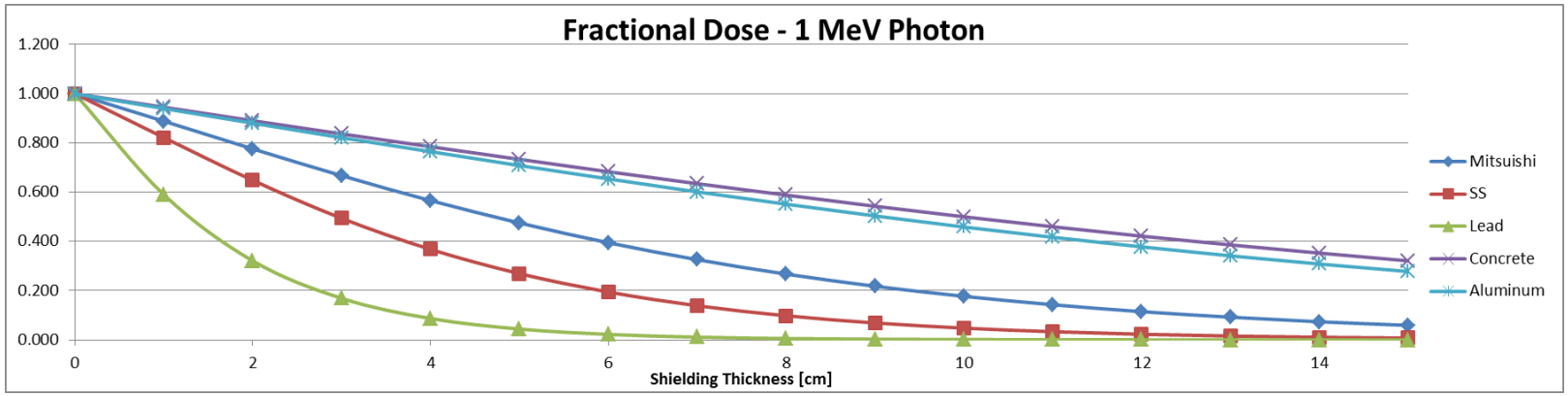

SLAB GEOMETRY

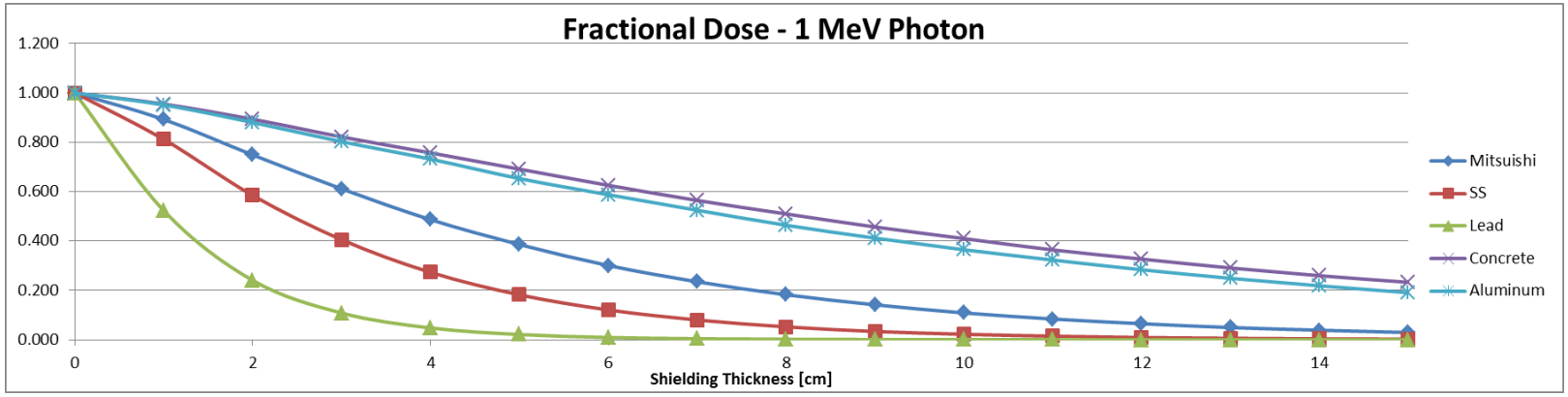

Gamma Dose_vs Shield Thickness

1.2 MeV Source

SPHERICAL GEOMETRY

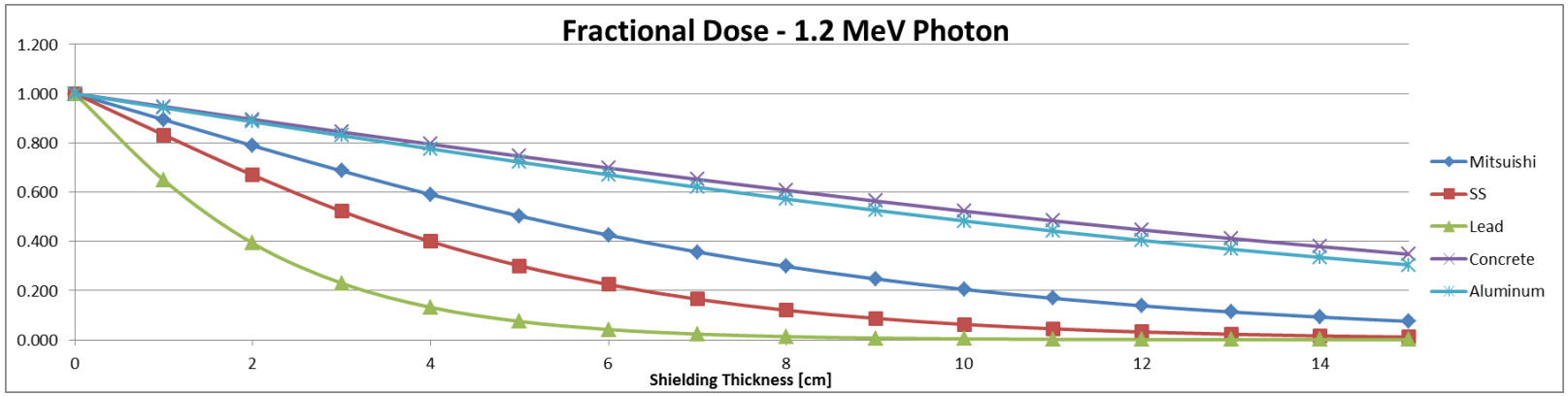

SLAB GEOMETRY

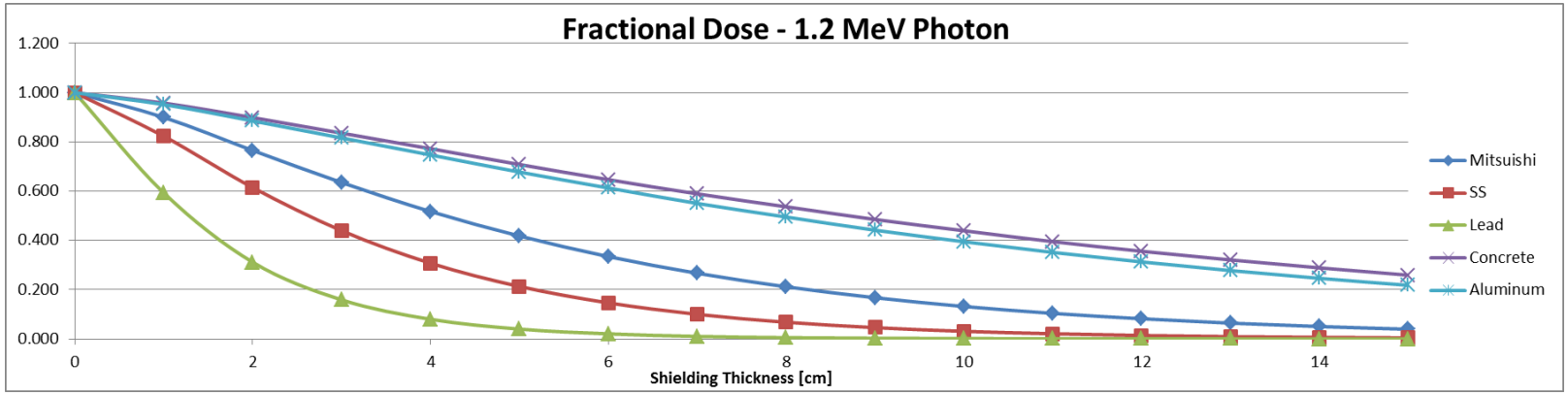

Gamma Dose_vs Shield Thickness

1.4 MeV Source

SPHERICAL GEOMETRY

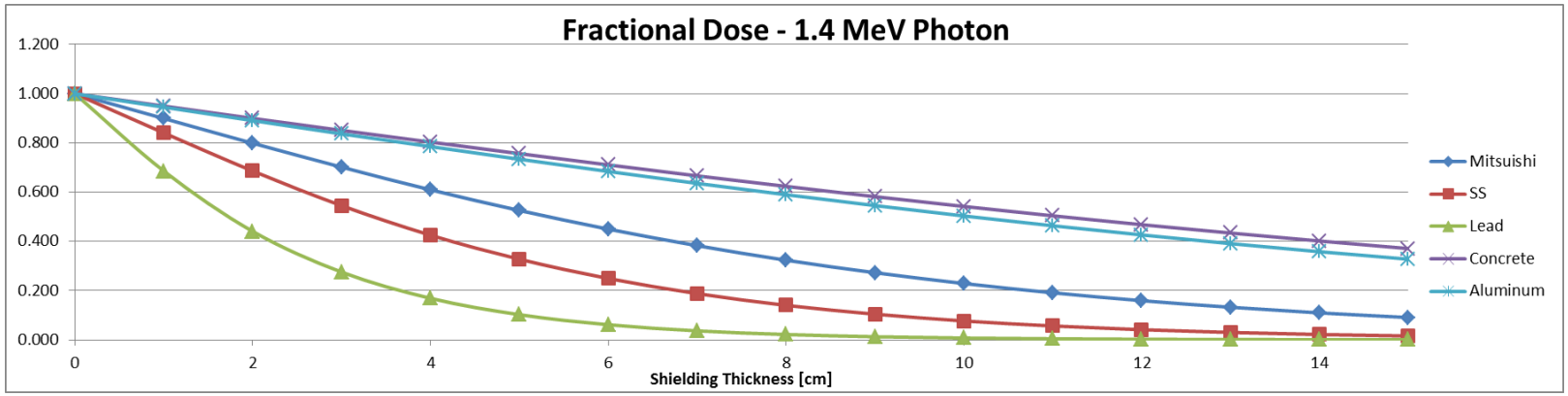

SLAB GEOMETRY

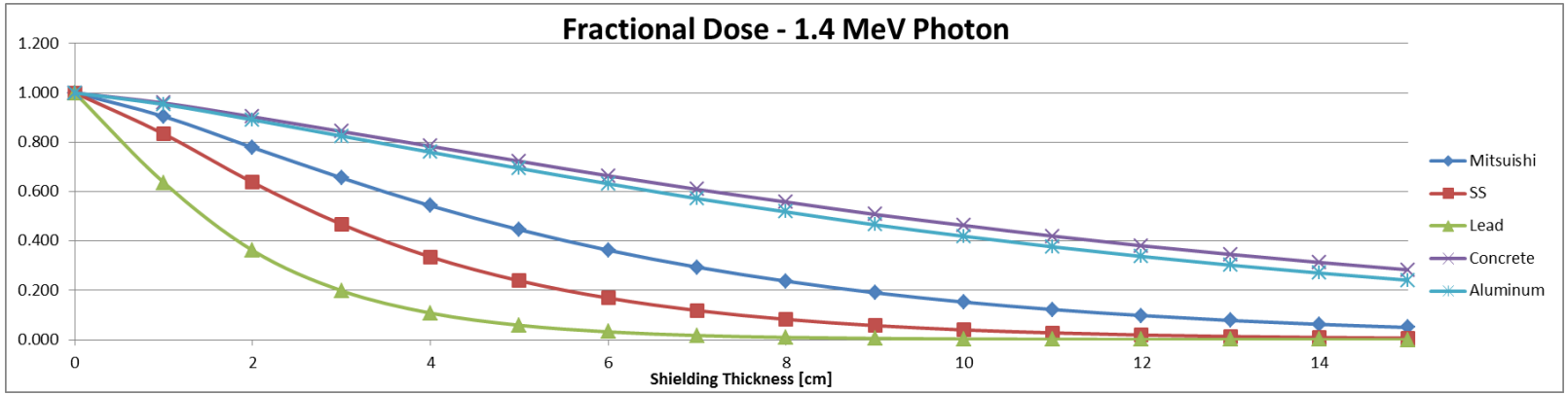

Gamma Dose_vs Shield Thickness

1.6 MeV Source

SPHERICAL GEOMETRY

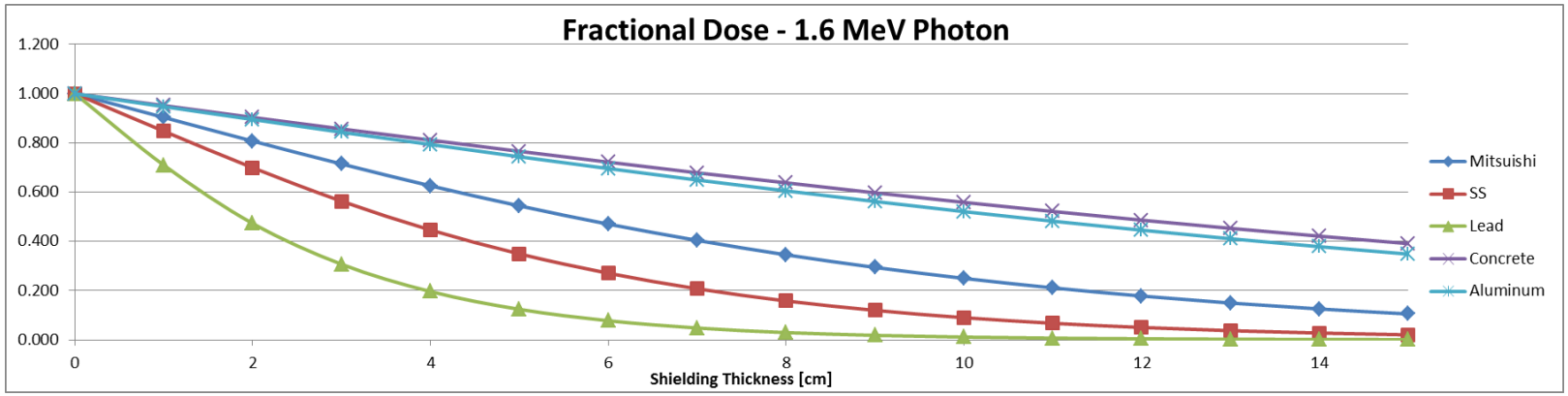

SLAB GEOMETRY

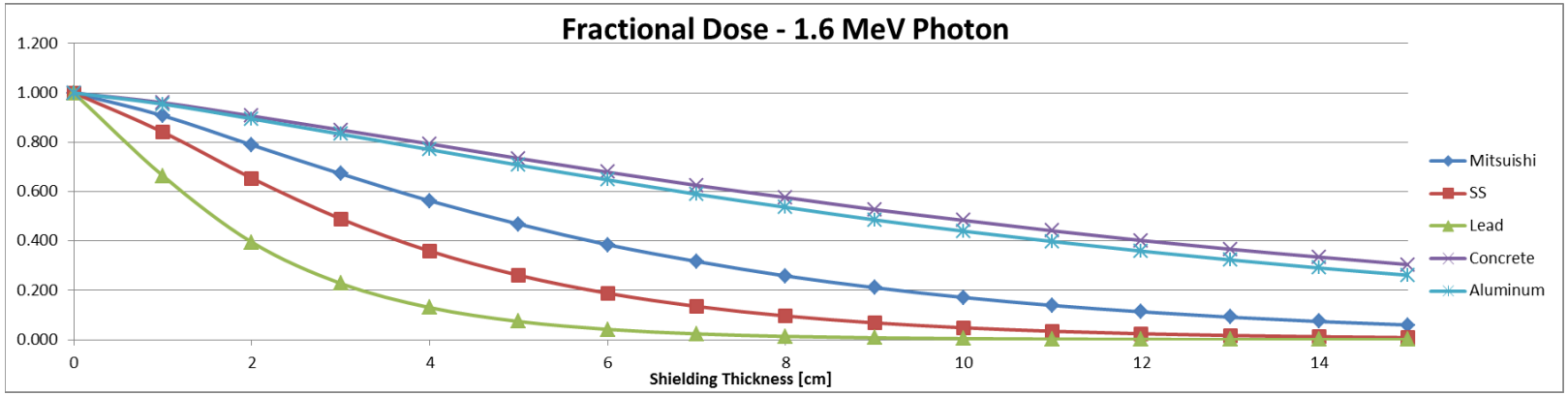

Gamma Dose_vs Shield Thickness_

1.8 MeV Source

SPHERICAL GEOMETRY

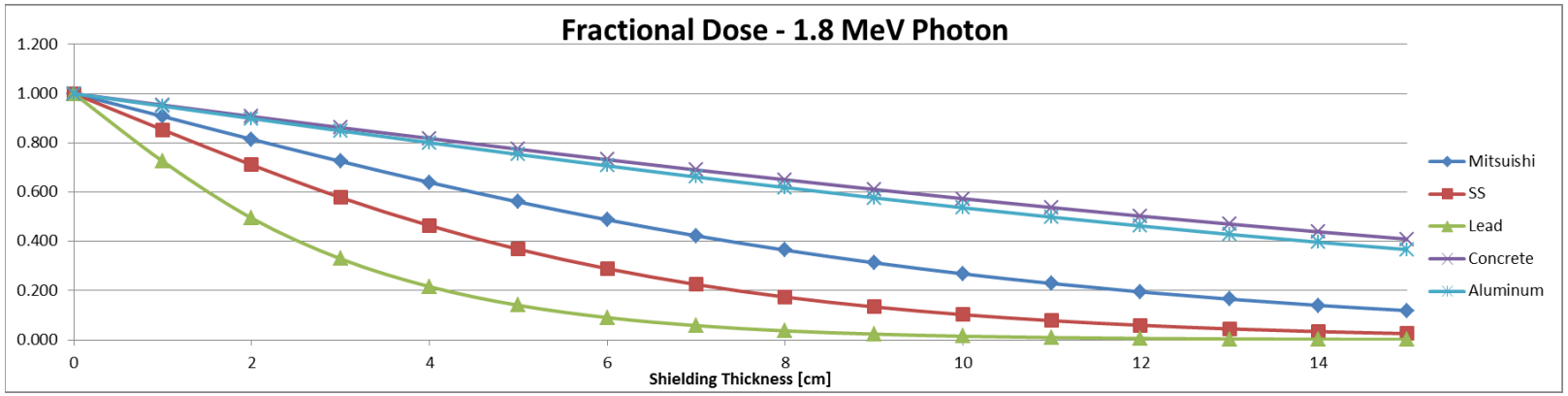

SLAB GEOMETRY

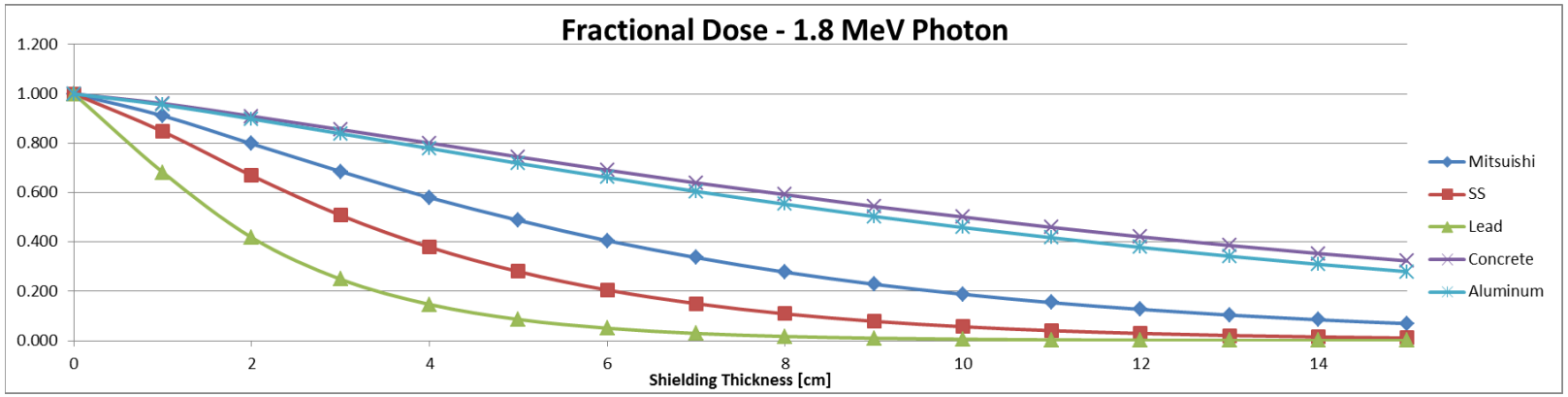

Gamma Dose_vs Shield Thickness

2 MeV Source

SPHERICAL GEOMETRY

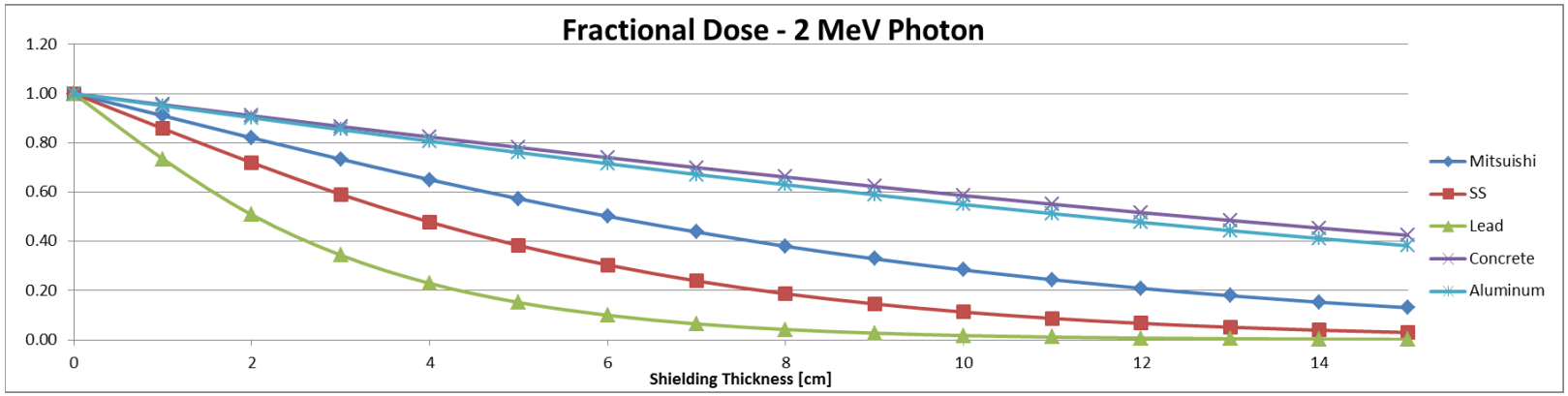

SLAB GEOMETRY

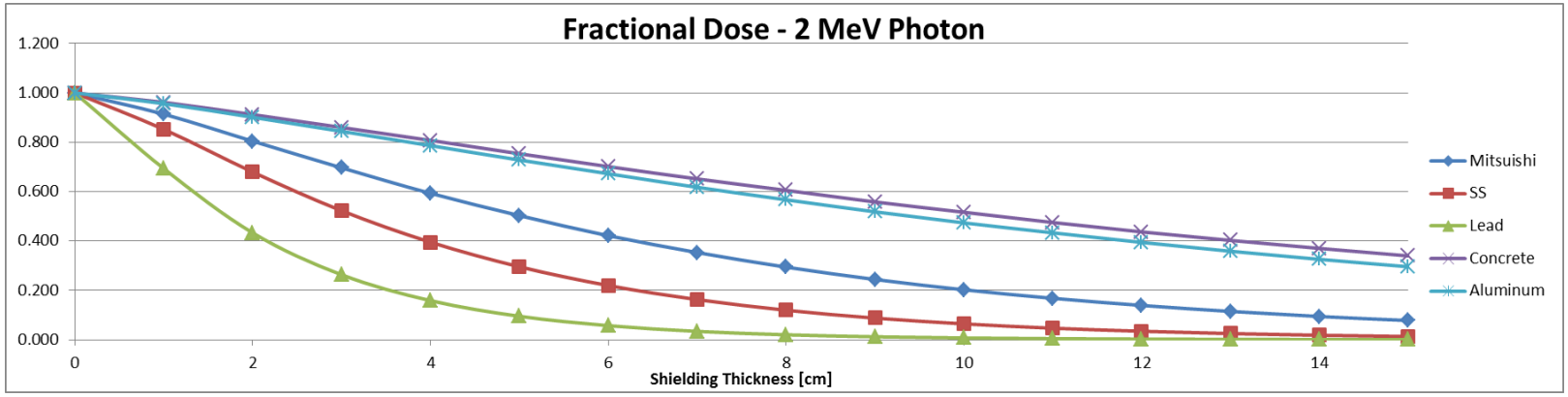

Neutron Dose_vs Shield Thickness

200 keV Source

SPHERICAL GEOMETRY

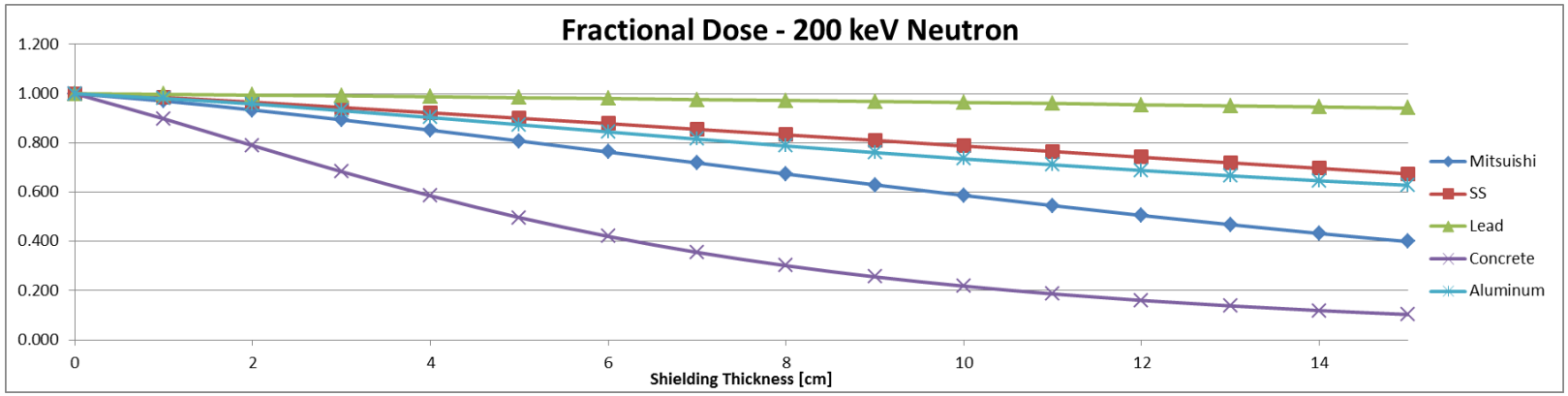

SLAB GEOMETRY

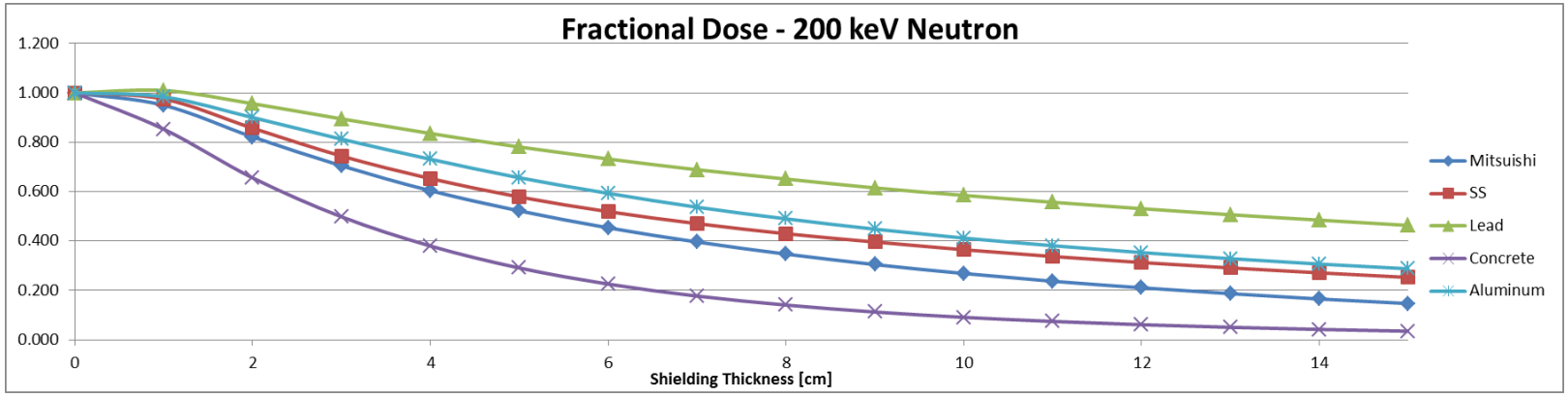

Neutron Dose_vs Shield Thickness

400 keV Source

SPHERICAL GEOMETRY

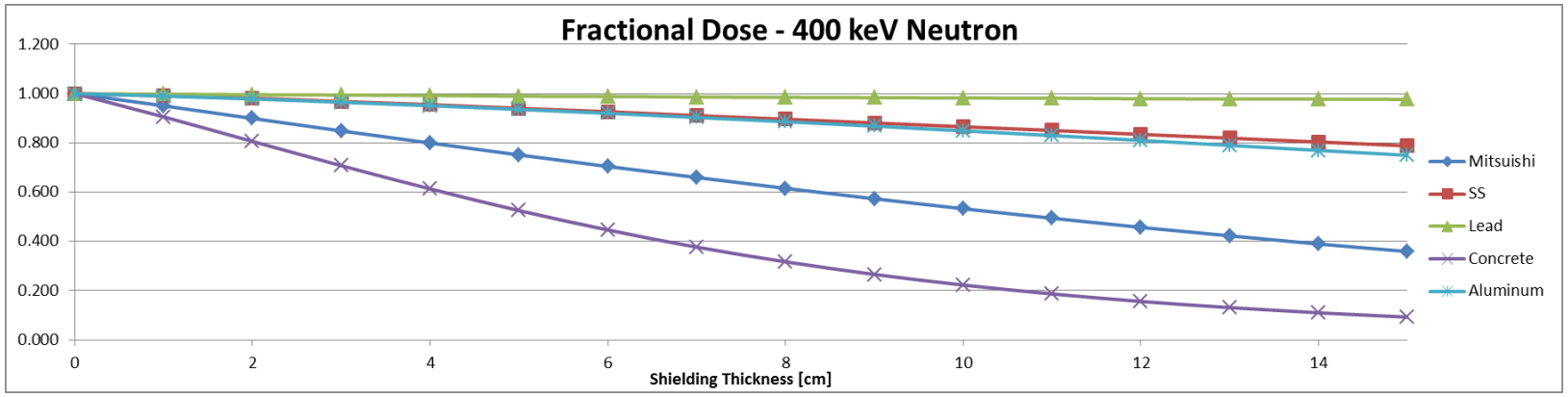

SLAB GEOMETRY

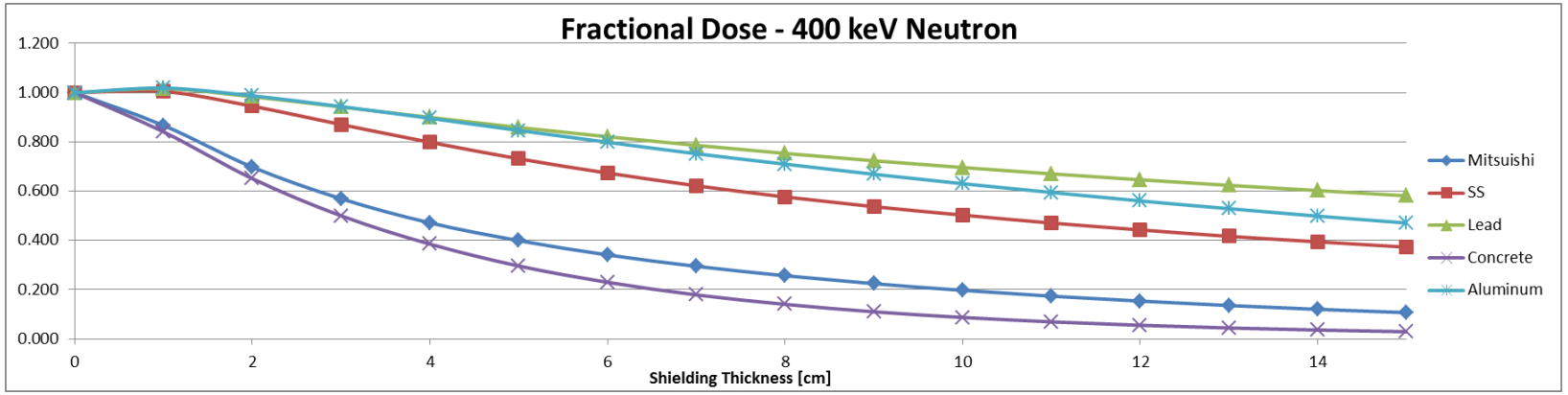

Neutron Dose_vs Shield Thickness

600 keV Source

SPHERICAL GEOMETRY

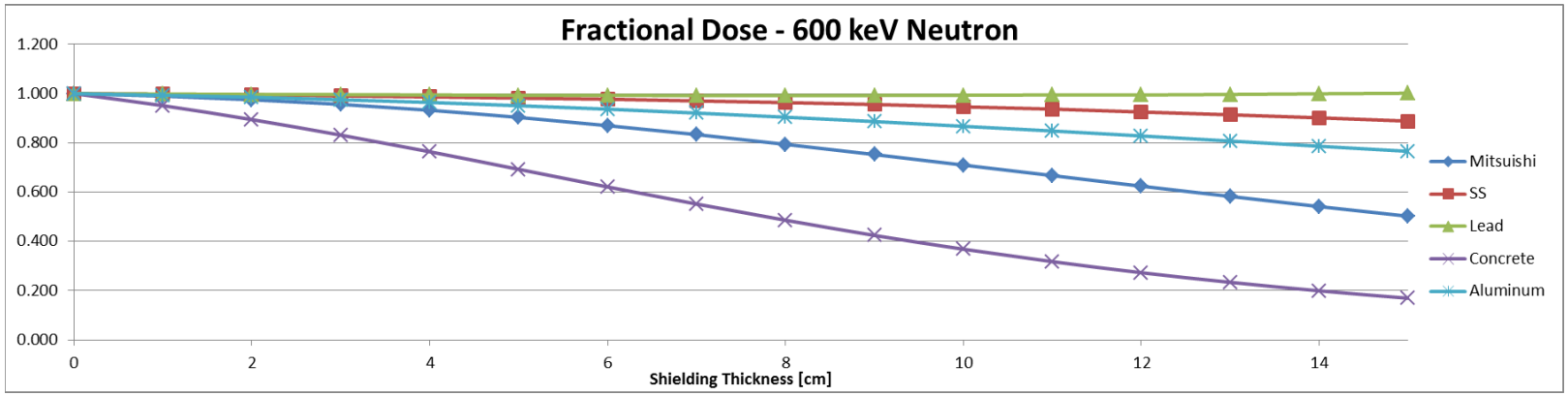

SLAB GEOMETRY

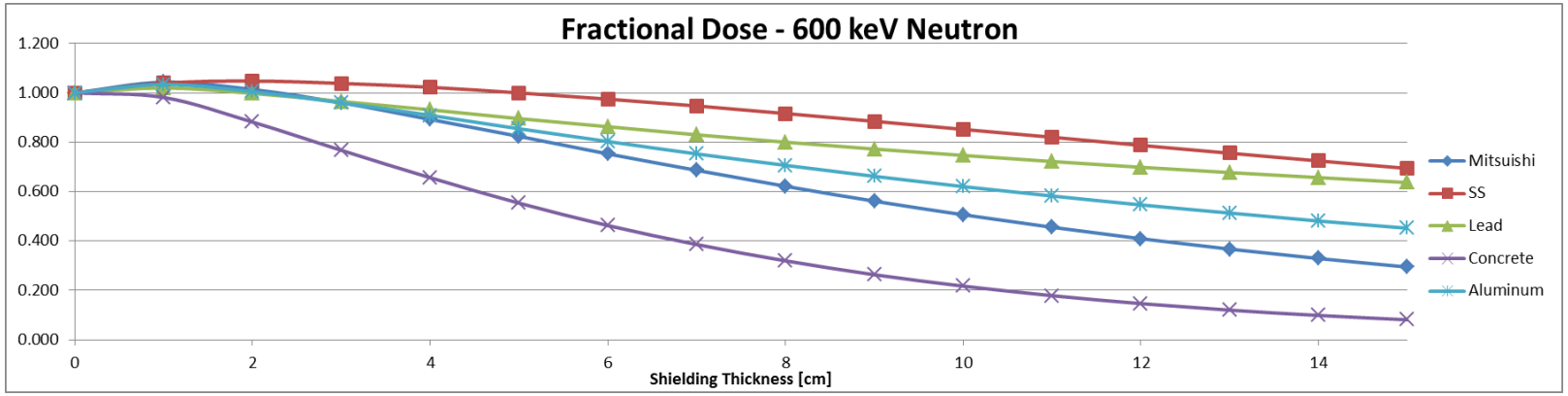

Neutron Dose_vs Shield Thickness

800 keV Source

SPHERICAL GEOMETRY

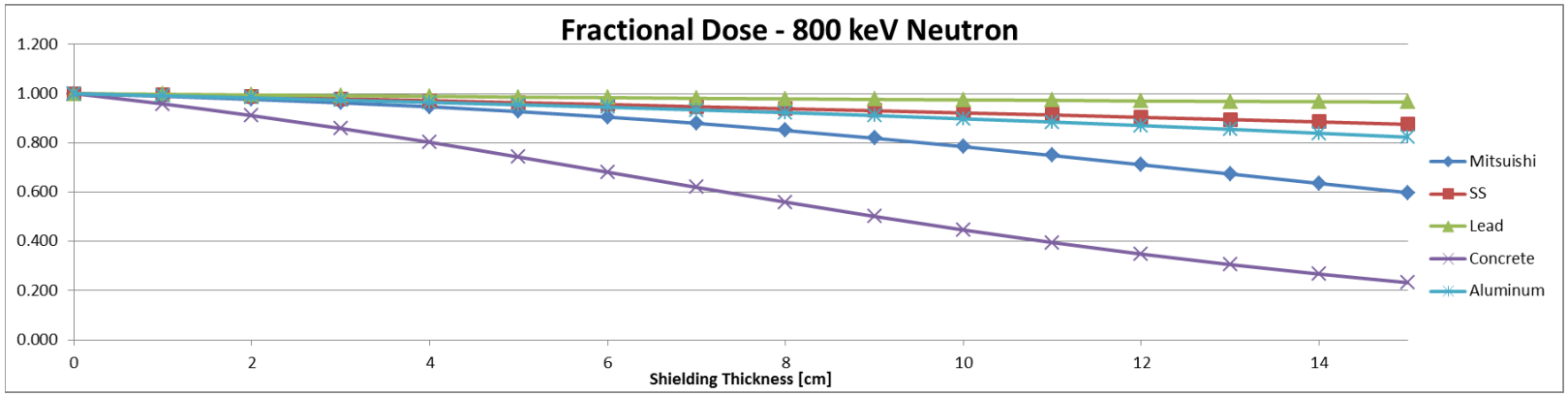

SLAB GEOMETRY

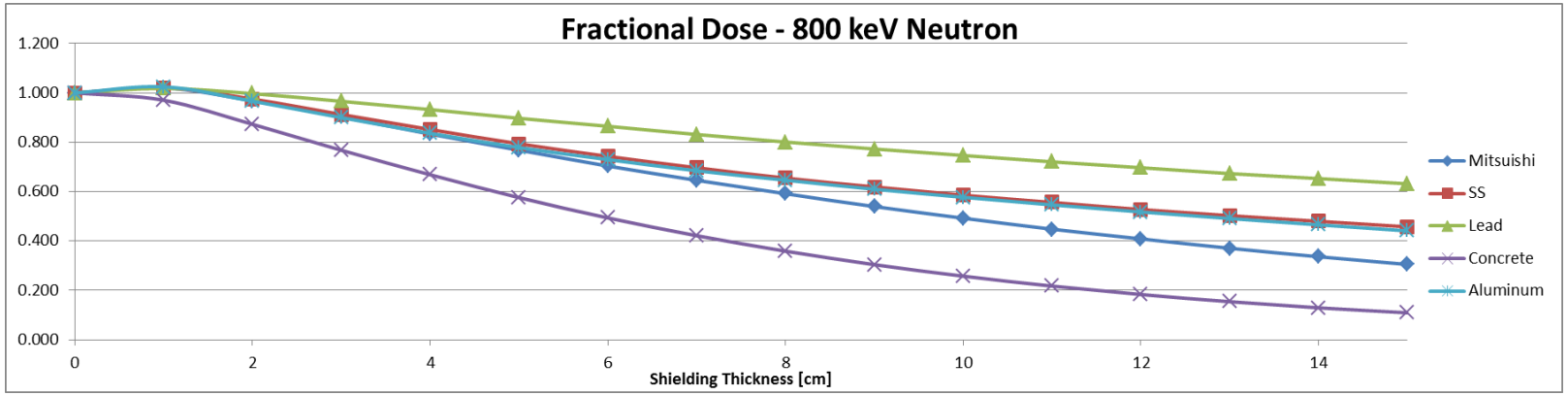

Neutron Dose_vs Shield Thickness

1 MeV Source

SPHERICAL GEOMETRY

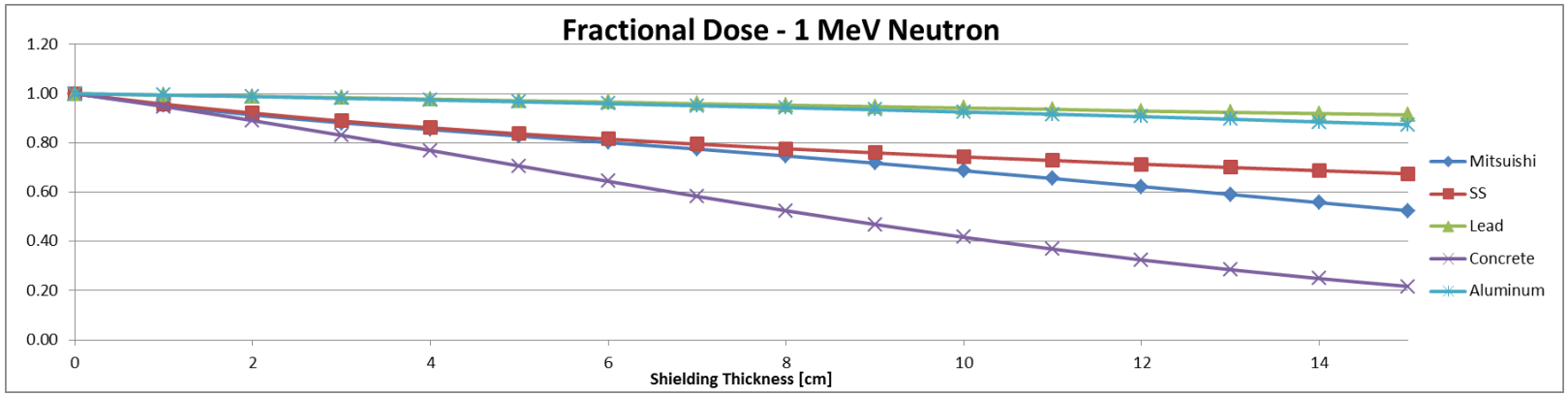

SLAB GEOMETRY

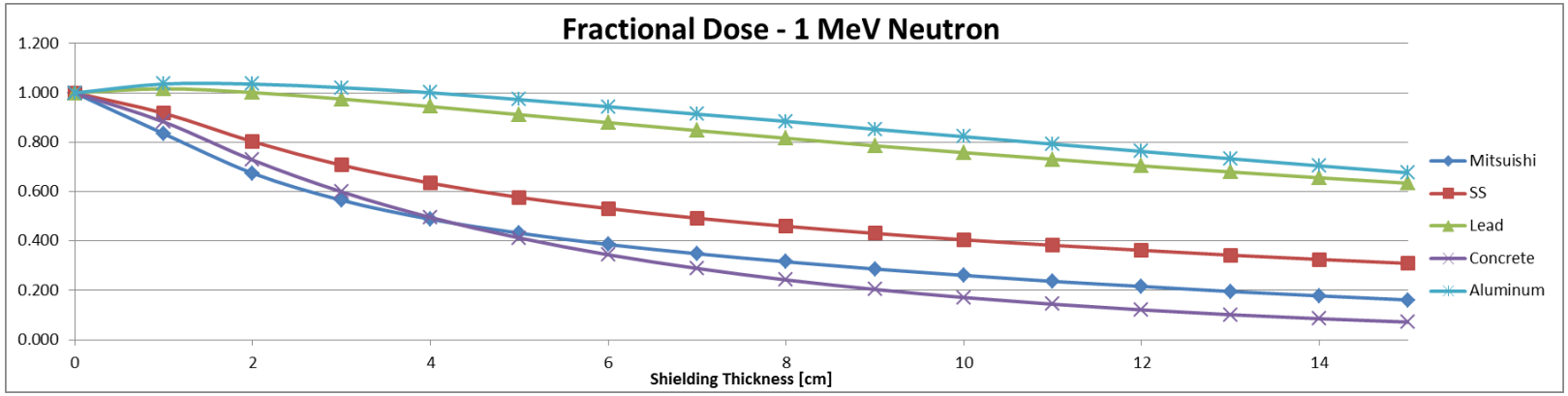

Neutron Dose_vs Shield Thickness

1.2 MeV Source

SPHERICAL GEOMETRY

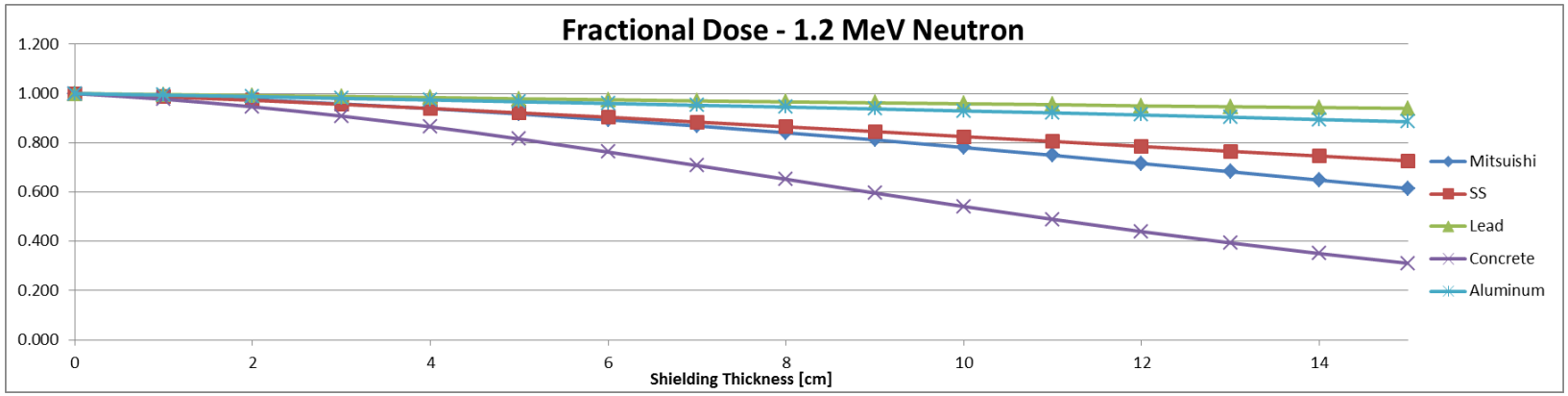

SLAB GEOMETRY

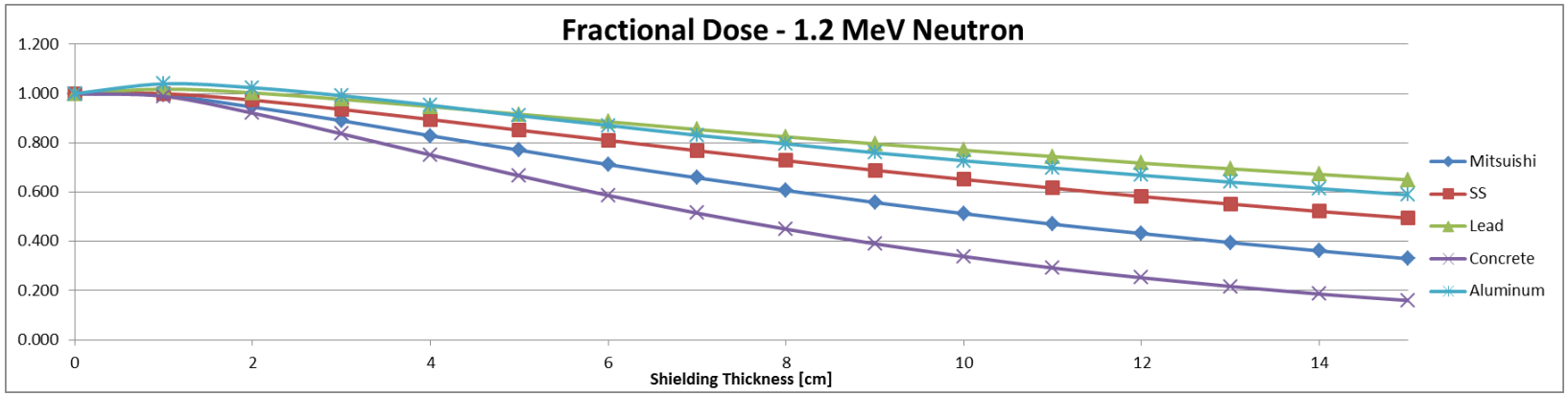

Neutron Dose_vs Shield Thickness

1.4 MeV Source

SPHERICAL GEOMETRY

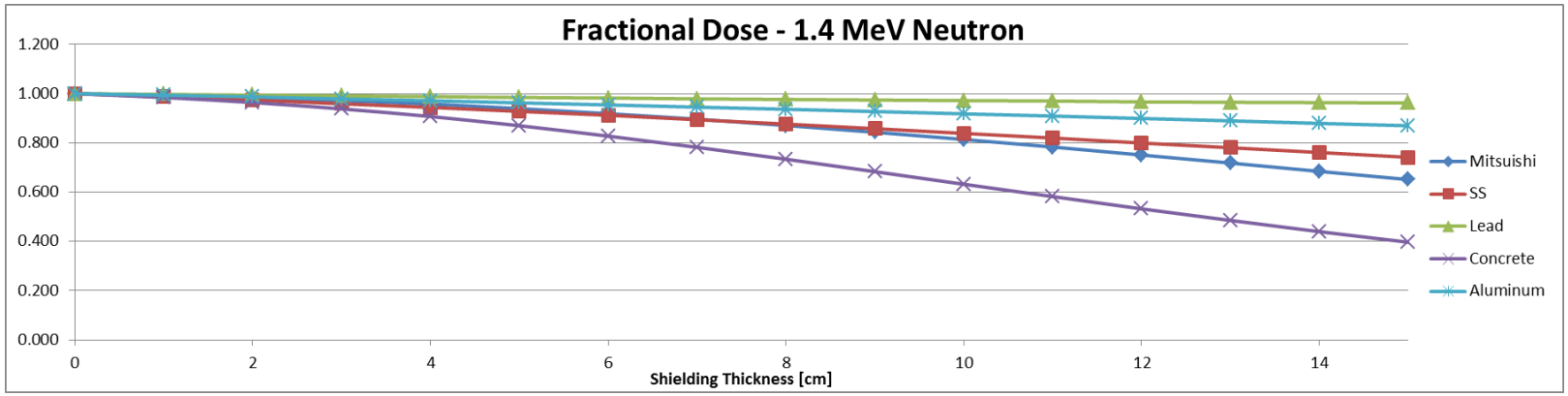

SLAB GEOMETRY

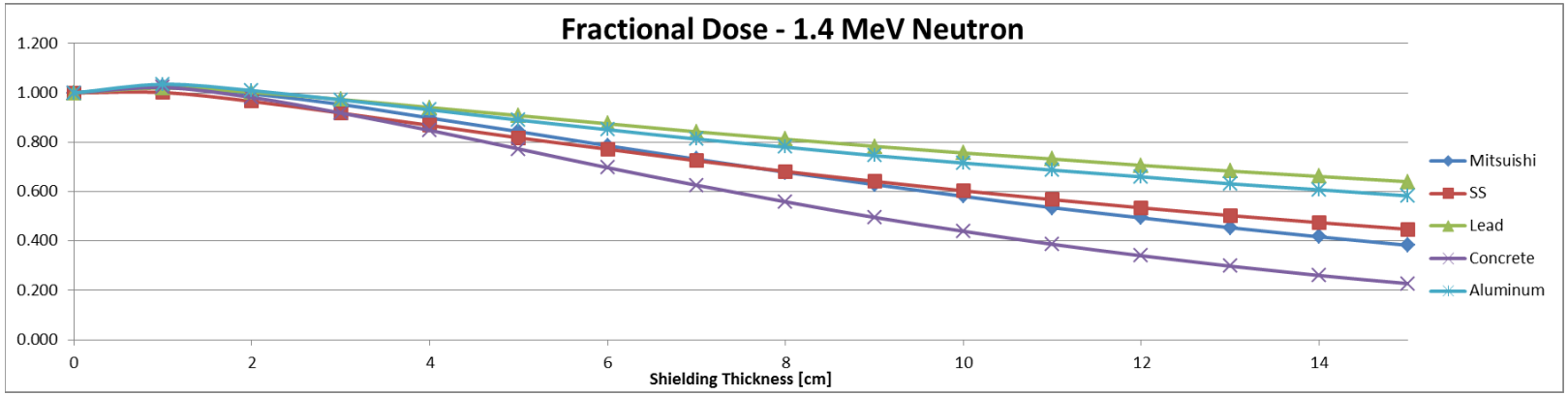

Neutron Dose_vs Shield Thickness

1.6 MeV Source

SPHERICAL GEOMETRY

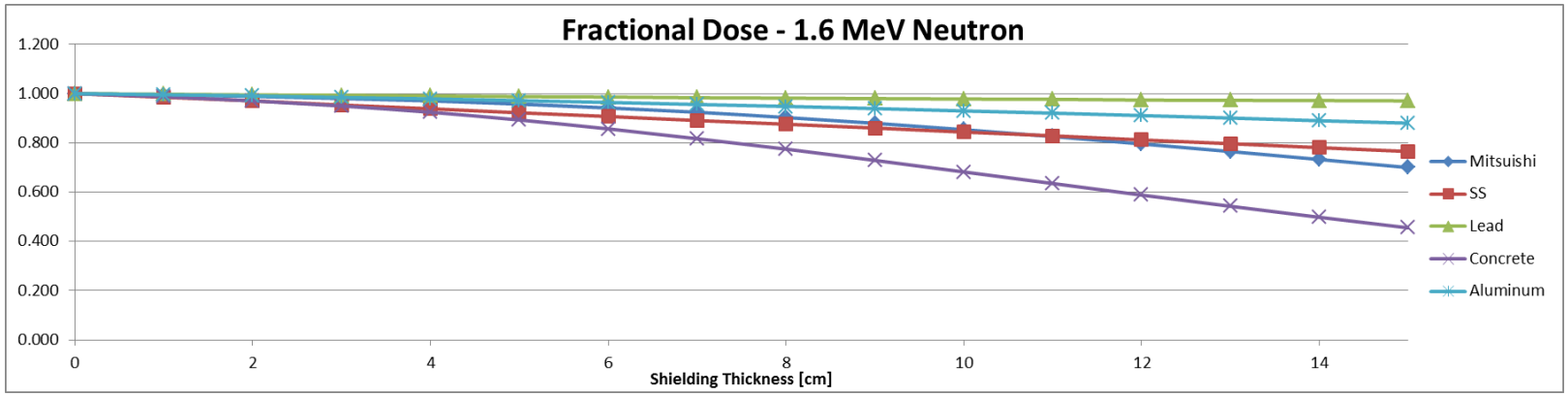

SLAB GEOMETRY

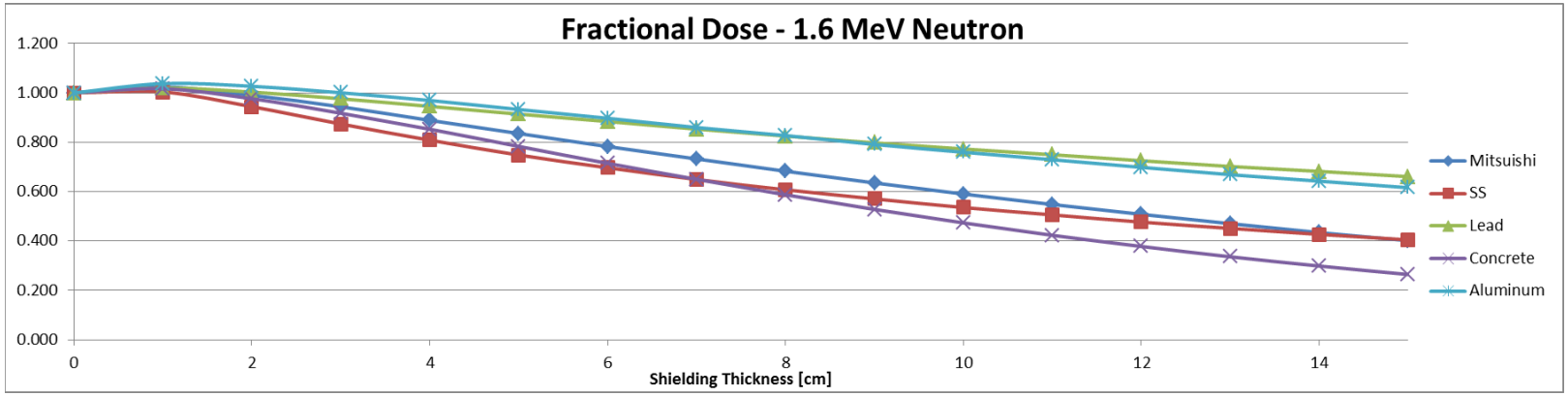

Neutron Dose_vs Shield Thickness

1.8 MeV Source

SPHERICAL GEOMETRY

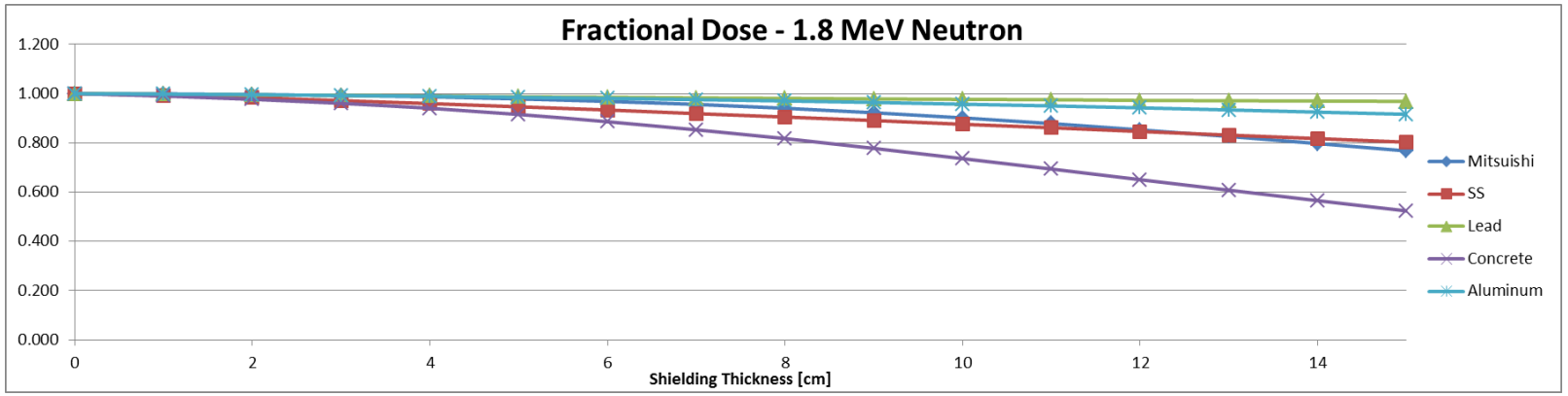

SLAB GEOMETRY

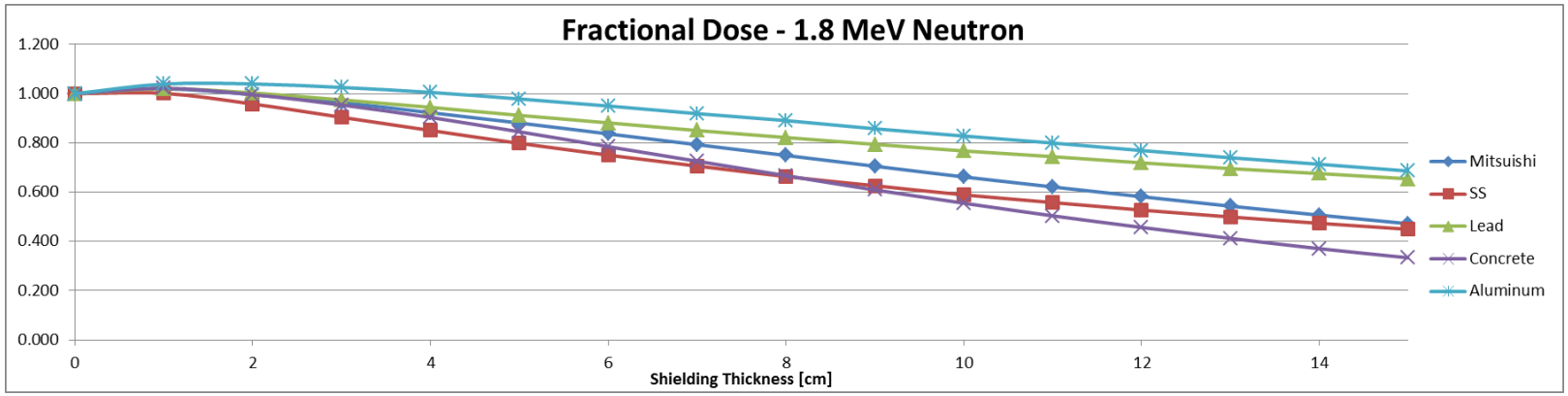

Neutron Dose_vs Shield Thickness

2 MeV Source

SPHERICAL GEOMETRY

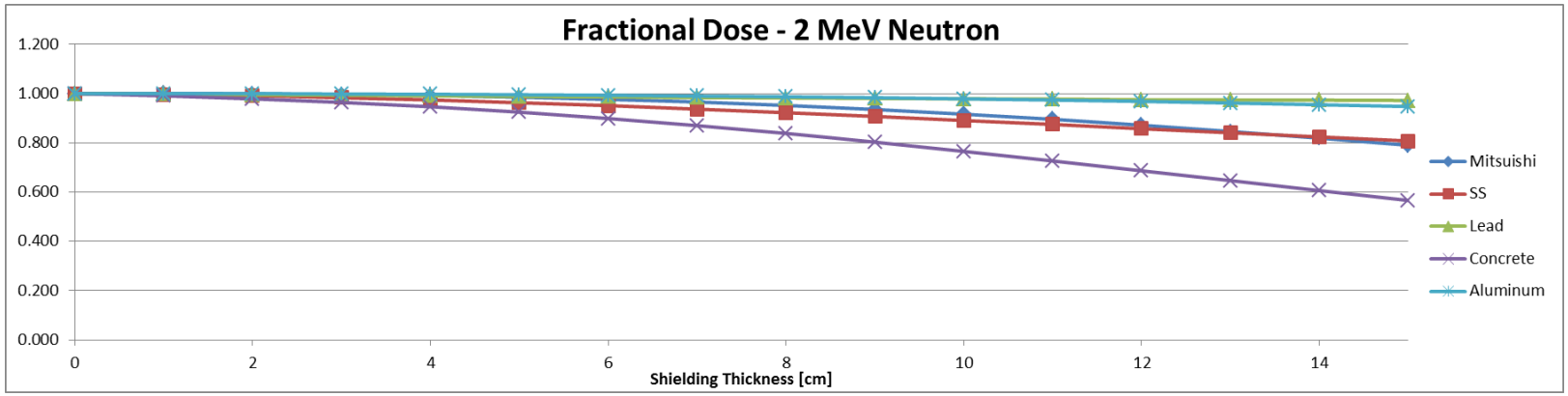

SLAB GEOMETRY

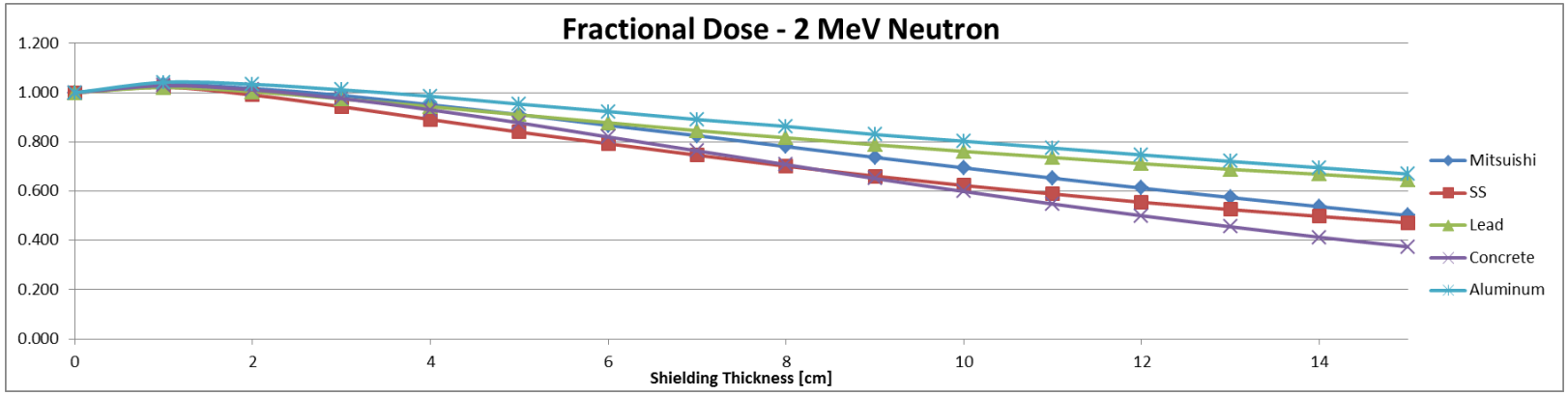

Neutron Dose_vs Shield Thickness

Fission Spectrum Source

SPHERICAL GEOMETRY

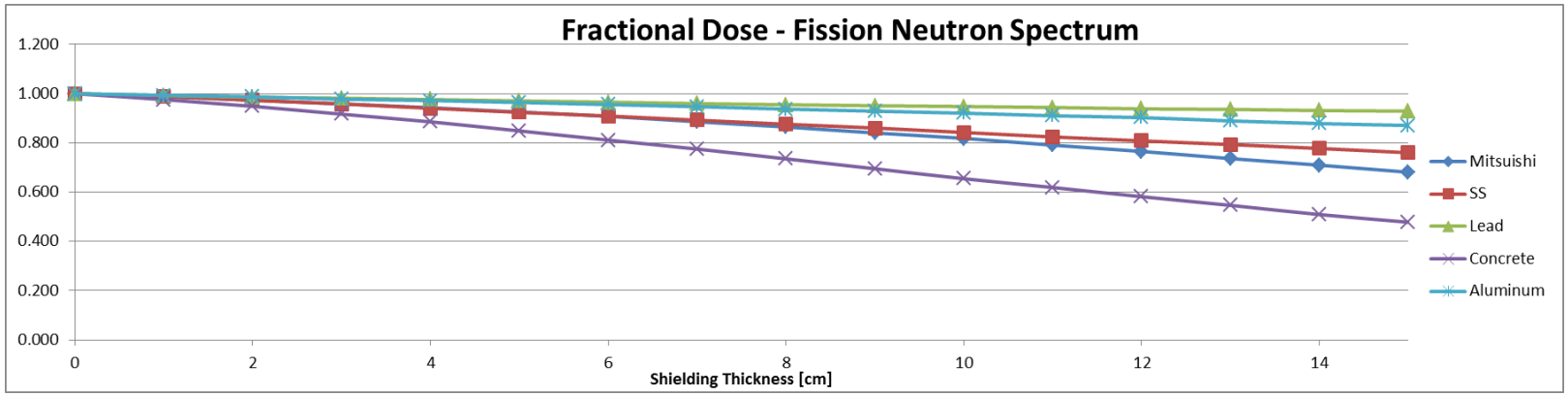

SLAB GEOMETRY